Characterization of Receptivity in Jet Flow Control

D. E. Parekh, A. B. Cain, C. N. Vaporean

McDonnell Douglas Corporation
St. Louis, Missouri 63166

31 October 1997
Final Technical Report

Prepared for:
Dr. Mark Glauser and Dr. James McMichael
UNITED STATES AIR FORCE
Air Force Office of Scientific Research
Bolling Air Force Base, DC 20332

REPORT DOCUMENTATION PAGE

Form Approved
OMB No. 0704-0188

1. AGENCY USE ONLY (Leave blank)	2. REPORT DATE	3. REPORT TYPE AND DATES COVERED
	31 October 1997	FINAL REPORT 5/94 to 5/97

4. TITLE AND SUBTITLE

CHARACTERIZATION OF RECEPTIVITY IN JET FLOW CONTROL

5. FUNDING NUMBERS

F49620-94-C-0029

6. AUTHOR(S)

D. E. Parekh, A. B. Cain, C. N. Vaporean

7. PERFORMING ORGANIZATION NAME(S) AND ADDRESS(ES)

McDonnell Douglas Corporation
Wholly-owned Subsidiary of The Boeing Company
P.O. Box 516
St. Louis, MO 63166-0516

8. PERFORMING ORGANIZATION REPORT NUMBER

9. SPONSORING/MONITORING AGENCY NAME(S) AND ADDRESS(ES)

AFOSR/NA
110 Duncan Avenue, Suite B115
Bolling AFB, DC 20332-0001

10. SPONSORING/MONITORING AGENCY REPORT NUMBER

11. SUPPLEMENTARY NOTES

12a. DISTRIBUTION/AVAILABILITY STATEMENT

Approved for public release; distribution is unlimited.

12b. DISTRIBUTION CODE

13. ABSTRACT *(Maximum 200 words)*

This report describes a combined experimental and computational investigation of the receptivity of incompressible and compressible jets to acoustic and fluidic perturbations. Receptivity is the mechanism by which external disturbances transfer energy to instabilities in the flow. The focus of this research is characterizing jet receptivity for a broad range of actuator and flow parameters. The numerical computations explore the influence of forcing amplitude, combined harmonic and steady blowing, actuator location, Mach number, and termperature ratio. Experimental investigations compare the effectiveness of various types of actuators and document the flow response to high amplitude forcing by a periodic fluidic actuator.

14. SUBJECT TERMS

Receptivity, flow control, jets

15. NUMBER OF PAGES

62

16. PRICE CODE

17. SECURITY CLASSIFICATION OF REPORT	18. SECURITY CLASSIFICATION OF THIS PAGE	19. SECURITY CLASSIFICATION OF ABSTRACT	20. LIMITATION OF ABSTRACT
Unclassified	Unclassified	Unclassified	UL

PREFACE

The work reported here was performed by McDonnell Douglas Corporation, a wholly owned subsidiary of the Boeing Company, in Saint Louis, Missouri, for the United States Air Force Office of Scientific Research, Bolling Air Force Base, Washington, DC, under Contract F49620-94-C-0029. The Air Force technical monitors for this program are Dr. James McMichael and Dr. Mark Glauser. The principal and co-principal investigators are Dr. David Parekh and Dr. Alan Cain. The authors express their thanks to Mr. Joseph Kroutil, Mr. Jeff Bellerose, and Mr. Jim Dunne for their critical assistance in conducting the experiments. Professor Ari Glezer and Dr. Val Kibens were instrumental in developing the actuator concepts considered in this program. The authors especially thank Professor Ed Kerschen for providing valuable guidance based on his related research on receptivity theory.

TABLE OF CONTENTS

LIST OF FIGURES

1. EXECUTIVE SUMMARY

In applications ranging from thrust vectoring to jet noise reduction, more effective and affordable flow control approaches are continually being sought. Additionally, the weight and mission requirements of many future aircraft severely restrict conventional approaches for jet flow control. Fundamental to developing effective alternative approaches is understanding the receptivity of jet flows to various types of control effectors.

This report describes a combined experimental and computational investigation of the receptivity of incompressible and compressible jets to acoustic and fluidic perturbations. Receptivity is the mechanism by which external disturbances transfer energy to instabilities in a jet flow. By harnessing these instabilities, one can exercise significant control over jet characteristics without resorting to a bulky, brute force approach. The efficiency of such alternative flow control approaches is determined by the coupling between the imposed disturbance and the flow being controlled.

The complex and multi-faceted aspects of these jet receptivity issues require a combined analytical, computational, and experimental research program for effective and efficient solution. The computational and experimental efforts described here are complemented by a related analytical effort, described in a separate report, by Dr. E. J. Kerschen of the University of Arizona.

The focus of this research is characterizing jet receptivity for a broad range of actuator and flow parameters. The numerical computations explore the influence of forcing amplitude, combined harmonic and steady blowing, actuator location, Mach number, and temperature ratio. Through comparisons with Kerschen's theoretical results, parameters governing the onset of nonlinearity are identified. Experimental investigations compare the effectiveness of various types of actuators and document the flow response to high amplitude forcing by a periodic fluidic actuator. Additionally, for the special case of a resonant wedge actuator, the dominant coupling mechanism is identified.

This effort has been directly linked with Air Force applied programs on Fluidic Injection Nozzle Technology (FLINT) and Fluid Mechanics of Screech (FLUMES). Consequently, this work has resulted in the transition of flow control approaches and computational methods to these applied programs. The most significant example of this transition is the recent demonstration of active mixing enhancement on a full-scale jet engine.

2. INTRODUCTION

New breakthroughs in flow control applications, such as mixing enhancement or thrust vectoring, will be made as we learn to harness a flow's natural instabilities. The control of a jet flow, by the selective introduction of flow-amplified instabilities, requires an understanding of how instabilities can and cannot be imposed on the jet. The key idea that addresses the issue of effective coupling in the forcing of instabilities is receptivity. **Receptivity** is the explicit determination of the coupling between external disturbances (environmental or man made) and the eigenmodes of the linearized disturbance equations. The exploitation of control is based on the ability to selectively and efficiently excite amplified eigenmodes that produce a desired outcome. The primary constraint in the receptivity determination is the idea that only imposed disturbances that match the frequency and wavelength of the desired amplified eigenmode effectively excite the instability modes. This concept of receptivity was first suggested by Morkovin (1969) in his transition work and reviewed by Reshotko (1976) with a major breakthrough in a formal solution given by Goldstein (1983). Significant progress on selected problems has been made in recent years as indicated by the review of Kerschen (1990). Related research on incompressible forced shear layers was conducted by Bechert and Stahl (1988).

This report describes a two-year investigation of the receptivity of incompressible and compressible jets to acoustic and fluidic perturbations. Significant progress in understanding the complex receptivity process requires a combined theoretical, computational, and experimental approach. This report presents a combined computational and experimental approach. A companion report by Dr. E. J. Kerschen (1996) of the University of Arizona (UA) details the theoretical part of this collaborative research.

Active control of jet flows has many military and civilian payoffs. Enhanced (or reduced) mixing, noise control (mixing can be an important part of this behavior), and

thrust vectoring are among the more obvious modifications of jet flow with important applications. Enhanced mixing is an important aspect of infrared signature reduction, reduction of combustion volumes, and reduction of jet noise particularly in an ejector nozzle system (where the effective exposed plume Mach number is reduced). There are a variety of methods by which active control of jet mixing can be achieved. For all such approaches it is important that the effectiveness (efficiency and reliability) of the given control technique be addressed. This work characterizes the coupling efficiency of selected excitation techniques for the jet mixing application.

The next section of this report discusses the complementary nature of the primary elements of this program and technology transition targets for this program. Subsequent sections present the key results of this program. The section on characterization of actuator effectiveness highlights experimental research focused toward determining the mode of coupling of a set of actuators to the jet flow and the sensitivity of the flow to key actuator geometric parameters. Numerical results focusing on the onset of nonlinearity and on the dependence of receptivity on flow and actuator variables are summarized in the section on simulation of forced jet receptivity.

3. PROGRAM OVERVIEW

This integrated research program is a multi-faceted exploration of receptivity for jet control. Theory provides simplified modeling concepts and is the best tool for developing and understanding parametric influences. Computations provide detailed information for selected cases and allow the domain of validity of modeling assumptions to be evaluated. Experiments are essential for validating analytical and computational results, and often lead to the discovery of additional physical mechanisms. Most importantly, the synergism between closely coupled theory, computations, and experiments has significantly enhanced the value of the overall research program.

The present program also benefits from leveraging related research programs. A set of previous and concurrent programs on active flow control at McDonnell Douglas and Georgia Tech sponsored by AFOSR, NASA, and IRAD (Internal Research and Development) has led to a family of actuator concepts whose receptivity to jet flows is considered here. This leveraging of related programs not only minimized the amount of hardware development required on this current program but also helped to select which of a myriad of actuator concepts would be worth exploring.

This effort has been directly linked with Air Force applied programs on Fluidic Injection Nozzle Technology (FLINT) and Fluid Mechanics of Screech (FLUMES). This tie of basic research to applications of Air Force relevance has helped to focus the fundamental issues considered and has provided a clear path for the transition of these research results. Consequently, this work has resulted in the transition of flow control approaches and computational methods to these applied programs. The most significant example of this transition is the recent demonstration of active mixing enhancement on a full-scale jet engine.

4. CHARACTERIZATION OF ACTUATOR EFFECTIVENESS

The central theme of the experimental portion of this work is to evaluate the jet flow's sensitivity to actuator type and placement. In providing a summary of key results, this section introduces the concept of a generalized actuator, highlights the sensitivity of jet response to placement and orientation of a pulsed fluidic actuator, and documents the acoustic field of a piezo-wedge actuator. Other results, which are not included in this summary, include the mapping of the time-dependent velocity field of a pulsed fluidic actuator. Additionally, to provide specific baseline data for evaluating computational tools, detailed pressure profiles in an axisymmetric supersonic shear layer were obtained for a range of Mach numbers corresponding to overexpanded, ideally expanded, and underexpanded flow conditions.

4.1 Concept of a Generalized Actuator

A wide variety of devices have been and will be developed for use as actuators in active flow control applications. To understand how a given device interacts with a flow, it is useful to categorize the different types of perturbations produced by that device. By examining actuators in this way, one can determine the essential elements of the device's interaction with a flow and thus be able to compare that device more accurately with other devices or improve it more readily. If one understands what type of perturbation is most effective in affecting a flow, one could design an actuator specifically to maximize that type of perturbation.

Take, for example, a cantilevered, oscillating blade interacting with a free shear flow. This device is characterized by the simple harmonic deflection of its surface yet has multiple components of interaction with the flow. As illustrated in Fig. 4.1-1, this device can produce acoustic, vortical, fluidic, and mechanical perturbations of the flow. The acoustic component results from the unsteady pressure field created by the motion of the blade itself. The vortical component can involve the generation of vorticity and/or the

reorganization of existing vorticity. The term fluidic refers to the notion that the motion of the blade propels fluid away from its tip much as the action of an oscillating rudder on a rowboat or a hand-held fan. This results in the blade providing a net source of momentum and a directed mass flow (without being a net source of mass). In contrast, devices that involve pulsed blowing would include a net source of both mass and momentum. Finally, the blade has a mechanical interaction with the shear layer as it periodically displaces the layer in space. For other devices, the generalized actuator concept would need to be extended to include thermal and electromagnetic effects.

Sorting out the different types of perturbations associated with a device would require a lot of detailed measurements, but some simple observations of the flow's sensitivity to the actuator's position can often lead to a qualitative determination of which excitation components are most important. In the case of the blade actuator, if it is moved a slight distance away from the shear layer, its interaction will be dominated by the acoustic and fluidic components. Even further away, the coupling between the actuator and the flow is primarily through the pressure field as a result of the acoustic perturbation generated by the device.

4.2 Experimental Apparatus

In these experiments, the flow source was a large storage tank system of dry air supplied at a nominal pressure of 600 psi. A computer-controlled digital valve maintained constant flow rate. The valve consisted of a binary sequence of parallel choked-flow orifices. For low-speed flows, a variable-speed centrifugal blower was used instead.

The flow conditioning system preceding rectangular nozzle models consisted of a round-to-rectangular contraction nozzle block of overall area ratio equal to 5.8:1, a series of screens and honeycombs, and an acoustic muffler. For some experiments, the flow exited from a rectangular, converging-diverging nozzle, with a design Mach number $M = 1.47$ and exit dimensions of 33.8 by 16.9 mm. Aspect ratio changes were

accomplished by adding an additional channel using straight-wall extension plates whose angular position could be varied to obtain nozzle exit aspect ratios (AR) over the range $2 \leq AR \leq 13$. Alternately, a fifth-order-polynomial-contour axisymmetric contraction was used to attach convergent axisymmetric nozzles to the flow plenum.

One of the control devices used as an actuator in this study operated at a resonance frequency of 5kHz. It consisted of a piezoelectrically driven wedge made of a high strength aluminum alloy oriented as shown in Fig. 4.2-1. The wedge was driven to oscillate resonantly in its second mode, and the wedge support struts were placed at the stationary nodes of the vibrating system. The actuator wedge tip was placed at a nozzle exit adjacent to the supersonic flow boundary, and moved in an arc tangent to a line in the streamwise direction. The tip of the wedge attained an amplitude of approximately 1mm at a resonance frequency of 5kHz.

For the 6.35-cm round nozzle, an array of 8 blade actuators were positioned symmetrically around the nozzle exit. Each actuator consisted of a thin stainless steel blade sandwiched between two slabs of piezoceramic material. These actuators had a resonant frequency tuned to 221 Hz. The phase of each actuator could be varied in increments of 90 degrees relative to the signal source. Thus, modal excitation from m=0 (symmetric) to m=4 could be approximated by this array.

Fluidic excitation was provided by directing pulsed air from a high pressure source or from the output of a piston-cylinder cavity. The pulsed excitation was directed through circular slit orifices on opposite sides of a 6.35-cm-diameter round nozzle. The excitation could be provided either in phase or out of phase in order to produce symmetric or antisymmetric excitation. Additionally, a 4.8-cm-diameter convergent round nozzle with internal slots was also used. Two opposing slots, each 90 degrees in circumferential extent, directed the pulsed fluidic excitation perpendicular to the internal nozzle flow. The slot location could be adjusted by switching to a different length nozzle termination.

Experimental measurements included flow visualization, time averaged pressure and temperature probe surveys, and acoustic measurements. A single-pass Schlieren system

was used for preliminary screening of the forcing configurations. This technique allows an excellent full space/time view of the flow. The flow visualization images were captured and recorded with a Panasonic 5000 video camera and a Sony BVW-75 BetaCam video recorder. To enhance visualization the flow is typically heated to 100°C or seeded with small amounts of CO_2. Pressure and temperature measurements were made with pitot, pitot-static, and aspirated-shielded-thermocouple probes. Hot-wire measurements were also made of the pulsed flow exiting the fluidic actuators.

4.3 Sensitivity to Pulsed Fluidic Actuator Location

Since the flapping mode ($m = \pm 1$) was generally most effective at generating vigorous large-scale mixing and could most easily be achieved with our available fluidic actuators, this study focused on the flapping mode. However, it should be noted that the higher-order modes are likely more effective at small-scale mixing than is the flapping mode.

The effect of mode $m = \pm 1$ forcing is to stretch the jet along the axis of symmetry and to squeeze it along the axis of antisymmetry, thereby resulting in an oval-shaped jet. This flapping motion is illustrated in the schlieren images of low-speed (20 to 50 m/s) jets excited by piezoelectric actuators (Fig. 4.3-1b), pulsed-jet actuators (Fig. 4.3-1c), and synthetic-jet actuators (Fig. 4.3-1d). In all three cases, actuators on either side of the x-z plane were operated 180 degrees out of phase, producing a flapping mode in the vertical direction.

The time-averaged evolution of the velocity and temperature field of the jet has been mapped out as a function of fluidic actuator frequency and amplitude and is discussed in some detail in a paper on jet mixing by Parekh *et al.* (1996a). A strong dependence of mixing effectiveness on frequency was established. This is primarily due to the instability amplification characteristics of the jet. Additionally, the frequency corresponding to the minima in the profiles depends on streamwise location, most likely due to variations in instability saturation location with wavelength. Not surprisingly, it was found that the largest temperature/velocity reductions in the near-field correspond to

higher frequencies than those for optimal far-field mixing. Mixing effectiveness also increases rapidly for injection ratios below 1% but quickly reaches an asymptotic limit at ratios around 2% for the external actuator configuration. The saturation of the jet response corresponds to significant velocity and temperature reductions and is achieved with very little mass injection. This fact suggests that mixing enhancement by this technique will be practical in many applications.

Along with the dependence on amplitude and frequency, the jet's response is sensitive to actuator position and orientation. Figure 4.3-2 provides a comparison of shear layer profiles corresponding to different positions of the external fluidic slot actuators powered by a piston-cylinder driver. The greatest reduction in centerline velocity and largest broadening of the jet results when the actuator is closest to the nozzle exit. This is not surprising since jet flows have highest receptivity to forcing at the trailing edge. The effectiveness of the actuator falls off more rapidly with downstream distance than with radial displacement. When the actuator is moved away from the jet exit, it is farther from the location of maximum receptivity and also does not benefit from as much cummulative amplification within the shear layer. In contrast, moving the actuator radially away from the jet has less of an effect since over several actuator slot heights the velocity of the pulsed flow exiting the actuator does not decay significantly.

The effect of actuator rotation relative to the jet axis is presented in Fig. 4.3-3. For the angles studied, it was found that a normal orientation provided the most mixing enhancement. In all three cases the actuator was rotated about its tip in order to keep the actuator the same distance from the shear layer.

Placing the actuator slot within the nozzle was much less effective than the external position for the pulsed fluidic excitation. Using baseline data for a slot location of 0.35 diameters upstream of the exit (from AFRL FLINT program; Parekh et al. (1996b)), data was obtained at an additional slot location to evaluate the sensitivity to slot distance from the trailing edge. The actuator air source in these cases was the pulsed high-pressure air supply. Figure 4.3-4 compares centerline velocity profiles for slot locations of 0.35 and

0.20 diameters upstream of the nozzle exit. Figure 4.3-5 compares the frequency response as a function of slot position, and Fig. 4.3-6 compares the amplitude response. Surprisingly, the slot position further from the nozzle exit had the larger impact on jet mixing. This is not consistent with the theoretical/computational results which indicate increased receptivity with increased proximity to the nozzle exit nor with physical intuition about this flow. One can conjecture explanations based on slight differences in the nozzle hardware or some tuning of the separated flow induced by the injected flow which could result in higher forcing amplitudes convected to the trailing edge for the more upstream slot configuration. However, to this point, the discrepancy has not been satisfactorily explained.

4.4 Characterization of Piezo-Wedge Actuator Acoustic Field

The effect of a piezoelectric wedge actuator on a compressible rectangular jet flow is evident in the centerline Mach number survey shown in Fig. 4.4-1. In both the unexcited and excited cases the potential core (Zone I) extends to a streamwise distance $x/H = 5$. The reference jet velocity decay rate follows a -1/2 power law for $x/H > 10$ and eventually increases to its asymptotic -1 slope. The excited jet centerline velocity profile also follows a -1/2 (Zone II) and -1 (Zone IV) decay slope, but the excitation moves these zones closer to the jet exit than in the reference case. Additionally, there is a region of minimal velocity decay (Zone III) not present in the reference jet. This zone corresponds to the onset of vigorous flapping in the jet where the rapid spreading of the jet causes a reduction in jet width in the perpendicular direction. This results in high-speed jet fluid being brought toward the center from the sides of the jet, thus minimizing the velocity decay in this region.

Effects of actuator frequency and amplitude are detailed by Parekh *et al.* (1996a). For the range of actuator amplitudes considered, the jet spreading was found to increase proportionately to the forcing amplitude, defined in terms of the acoustic perturbation pressure. The forcing amplitude was set by measuring the sound pressure level on the jet

centerline at 5 nozzle heights downstream. In this work the objective was to explore whether the acoustic field of the actuator could account for the sensitivity of the jet flow to actuator position as indicated in Fig. 4.4-2. Even though the difference in actuator position is more than half a nozzle height in streamwise position, the differences in the jet profiles at X/H = 20 are very slight.

A traversing B&K 4135 microphone was used to measure the acoustic field generated by the piezoelectric wedge actuator isolated in a quasi-anechoic chamber. Figure 4.4-3 presents a polar map of the sound pressure level for a fixed excitation voltage, Fig. 4.4-4 provides the corresponding phase map. The phase measurements are referenced to the electrical signal driving the piezoelectric elements. Figures 4.4-5 and 4.4-6 provide information about the variation of the acoustic field with excitation voltage level (denoted in arbitrary but scaled units on the plots). Finally, a typical acoustic spectrum is included in Fig. 4.4-7. From this plot, it is clear that the fundamental forcing frequency dominates its harmonics by over 30 dB. Since the acoustic amplitude is relatively constant for small distances away from the actuator, it would make sense for the jet response not to vary significantly with modest changes in actuator position if the coupling between this resonant device is primarily acoustic receptivity at the nozzle lip. The observation of linear scaling of jet spreading with acoustic perturbation amplitude and the noticeable impact of as little as 2 dB difference in acoustic forcing amplitude (Parekh *et al.*, 1996a) also suggest that the important coupling parameter is acoustic.

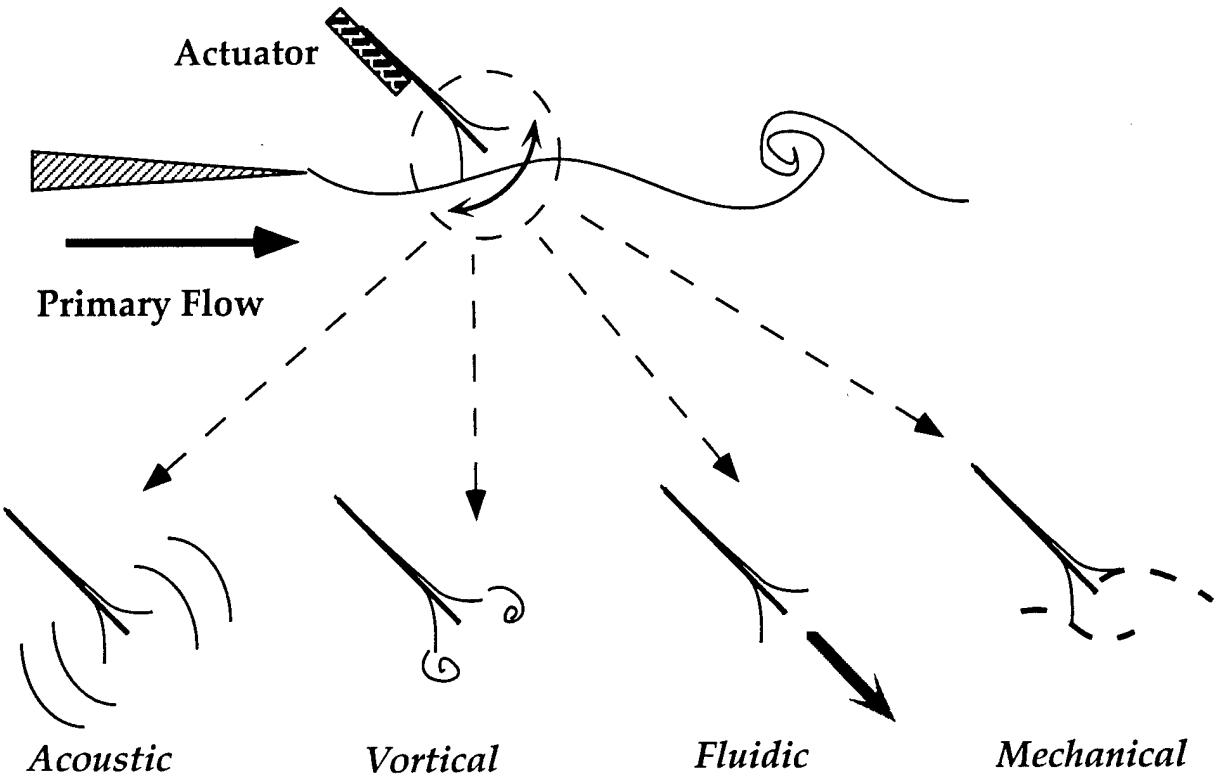

Figure 4.1-1. Classification of excitation sources.

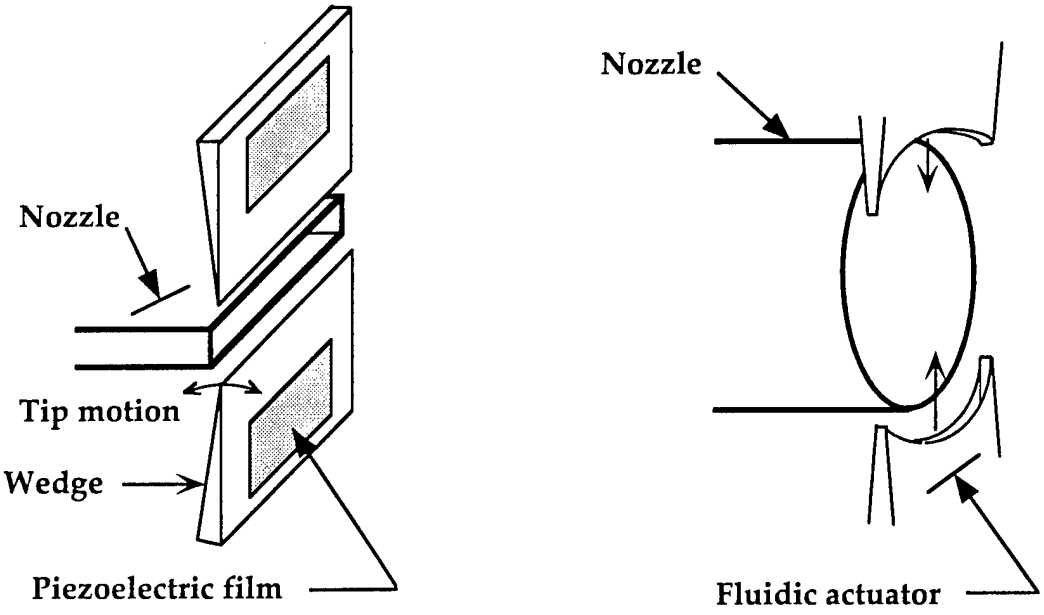

Figure 4.2-1. Schematic of nozzle-actuator configurations.

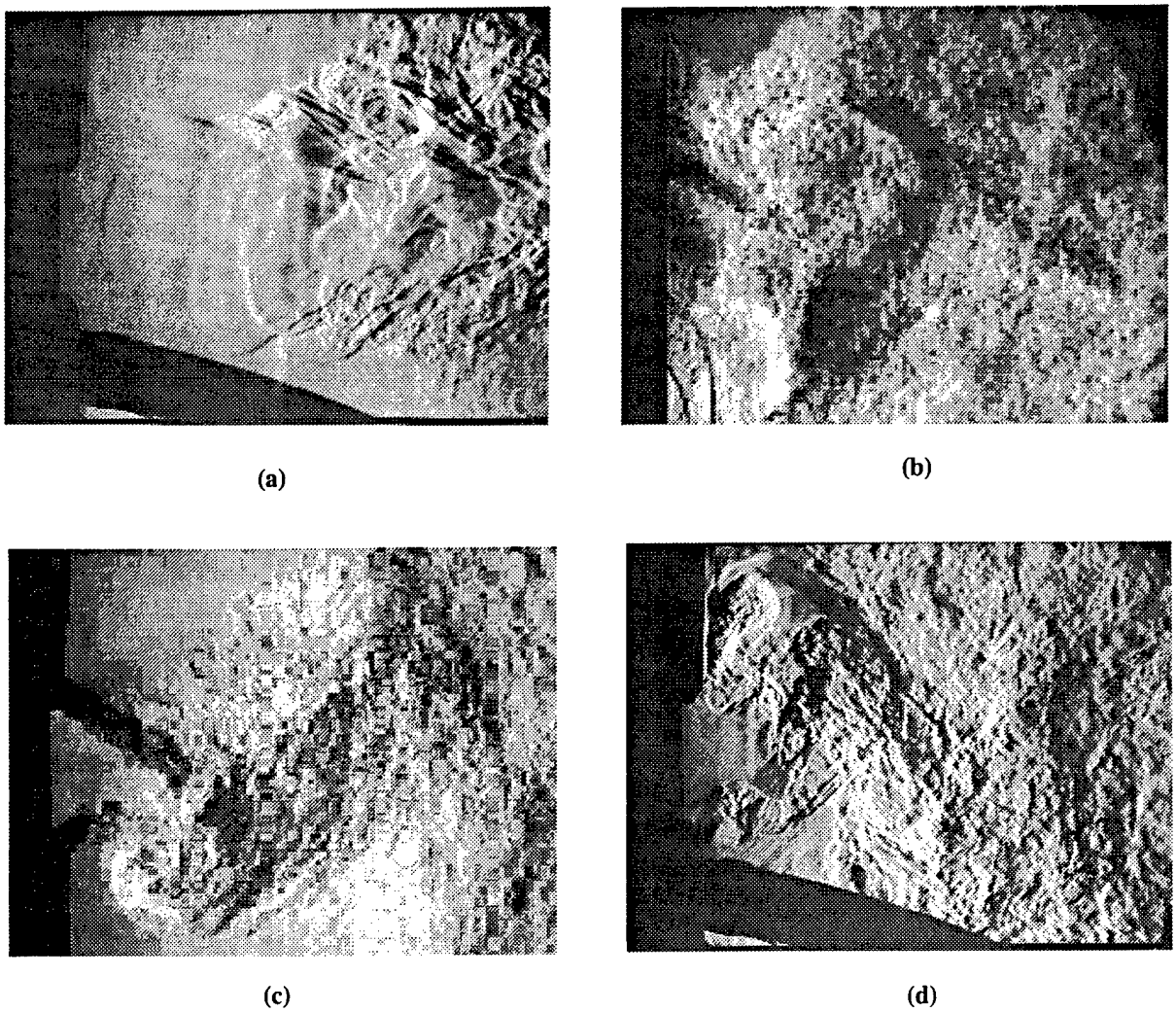

Figure 4.3-1. Schlieren visualization of typical round jet response to m = +/-1 mode excitation from various sources: (a) no excitation, (b) array of 8 piezoelectric blade actuators surrounding nozzle, (c) dual pulsed jets, and (d) dual synthetic jets.

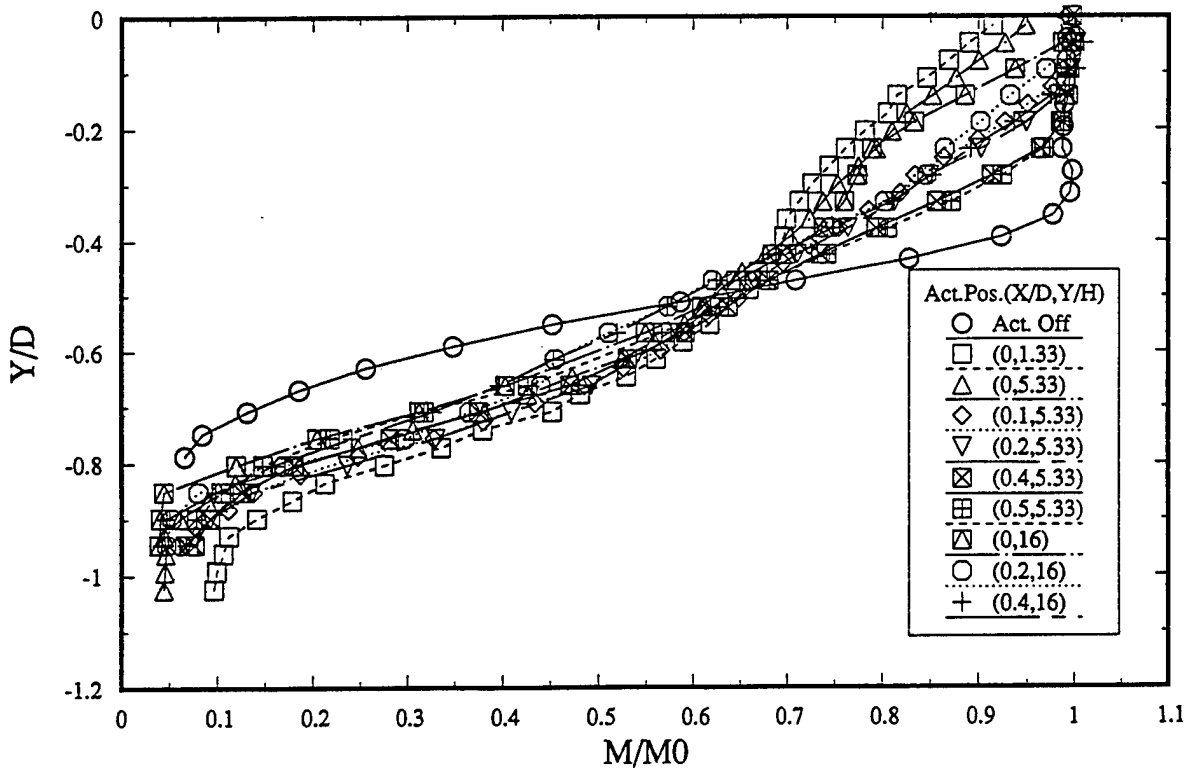

Figure 4.3-2. Transverse shear layer profiles for a single external piston-cylinder actuator at different positions. Primary jet velocity is 30 m/s with a constant amplitude excitation at a frequency of 120 Hz. Actuator position is measured from the nozzle lip. D is the jet diameter (63.5 mm), and H is the actuator slot width (1.2 mm).

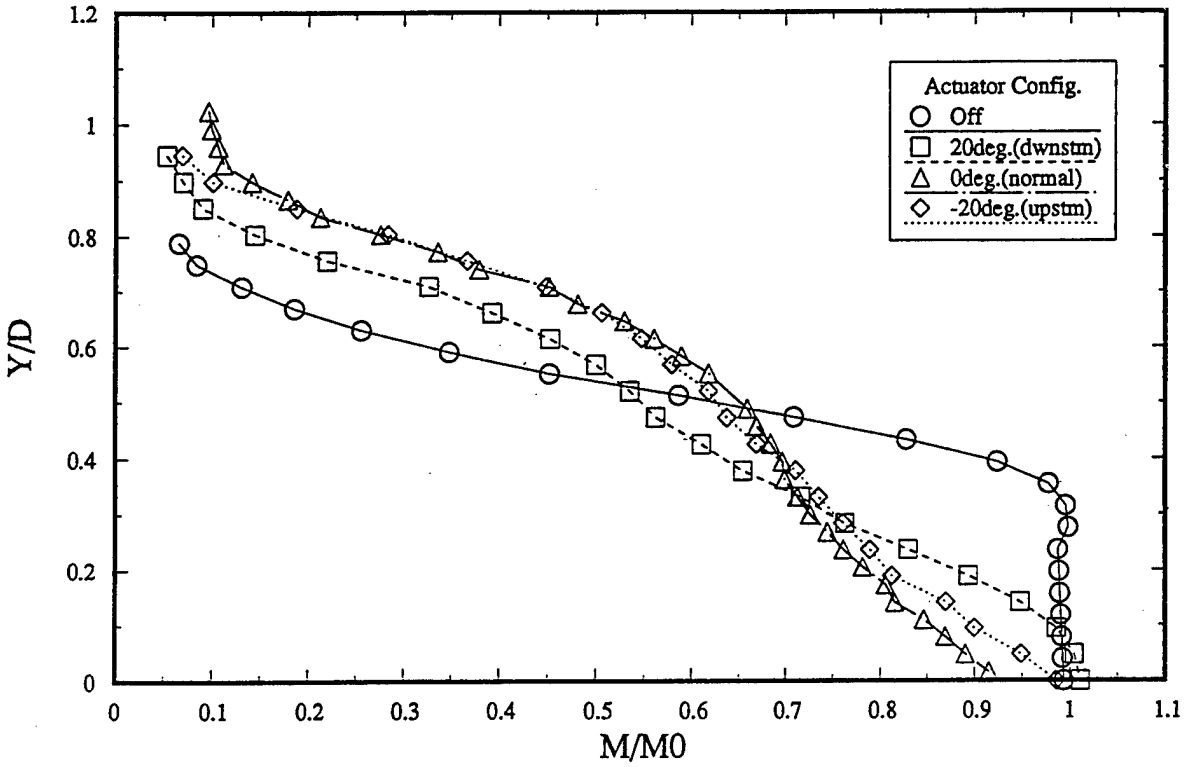

Figure 4.3-3. Transverse shear layer profiles for a single external piston-cylinder actuator at different angles relative to the primary flow. Primary jet velocity is 30 m/s with a constant amplitude excitation at a frequency of 120 Hz. Actuator orientation is measured relative to the jet normal such that 0-degree orientation corresponds to the actuator being perpendicular to the jet flow as shown in Fig. 4.2-1.

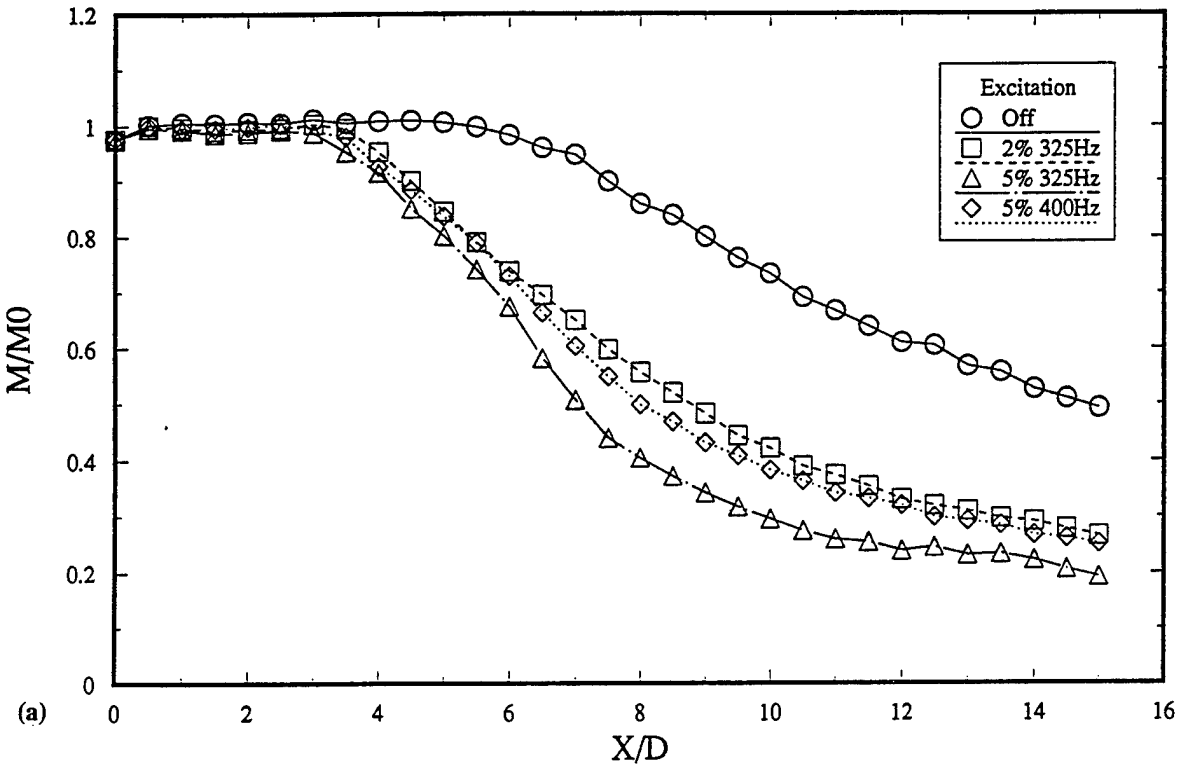

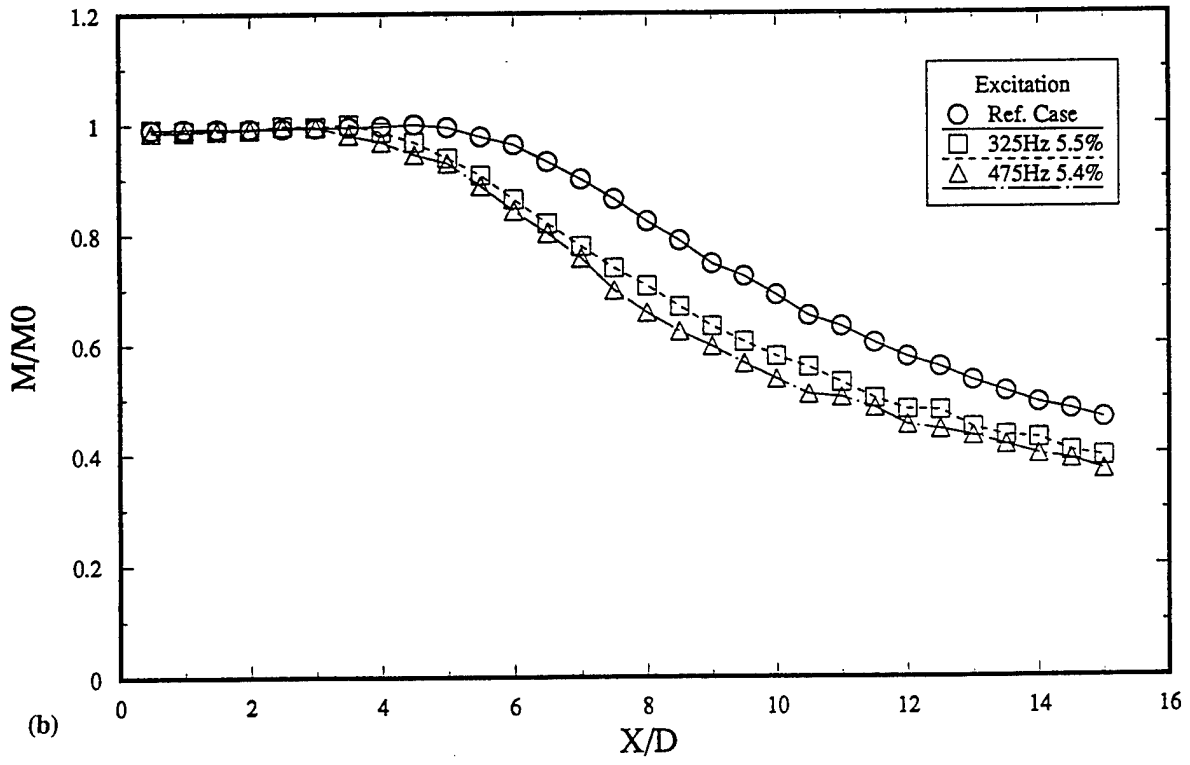

Figure 4.3-4. Centerline velocity profiles for axisymmetric nozzle with internal pulsed excitation slots at (a) 0.35 and (b) 0.20 diameters upstream of the nozzle exit. In both cases, jet exit velocity is 80 m/s.

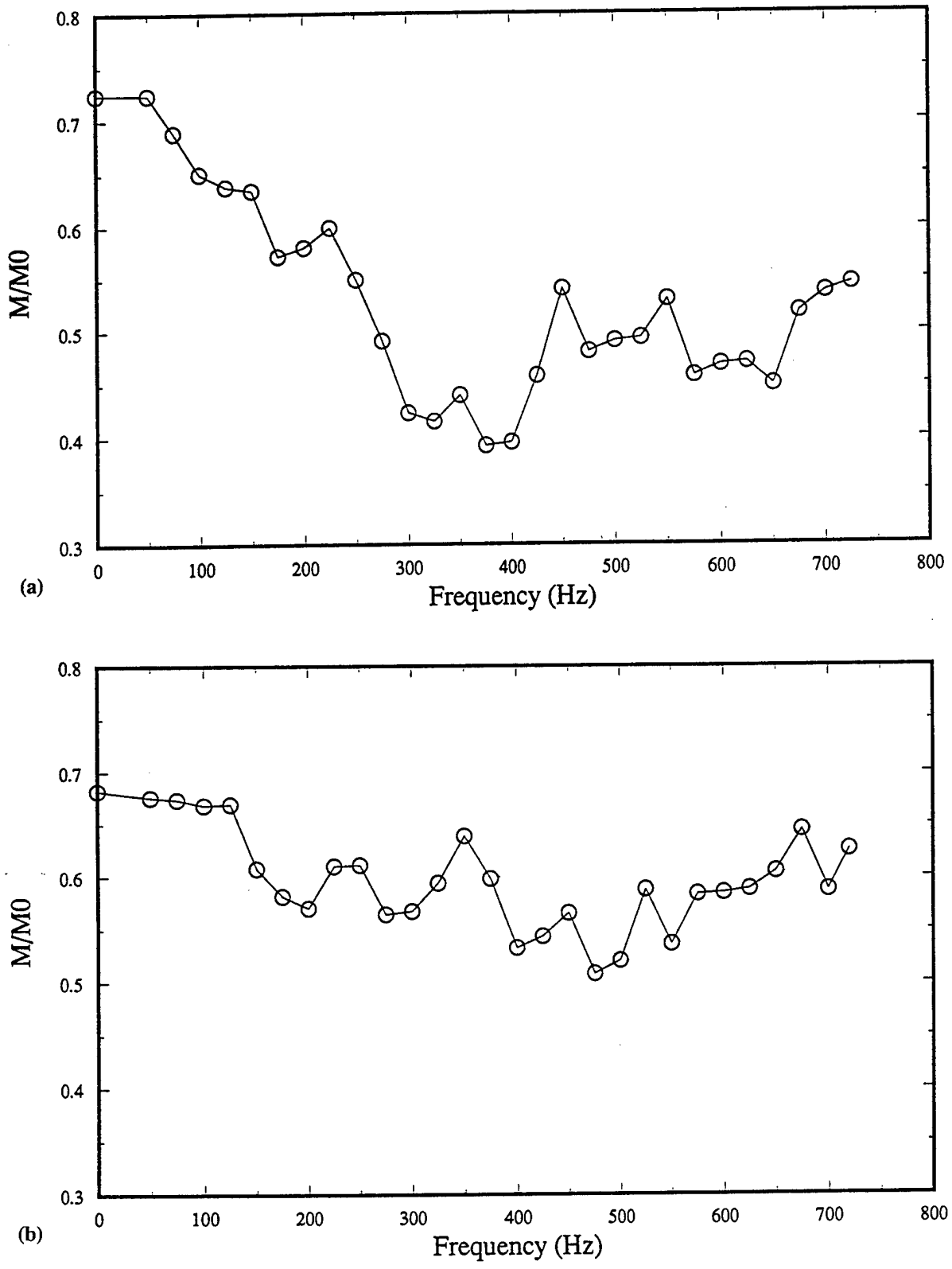

Figure 4.3-5. Centerline velocity at X/D = 10 as a function of excitation frequency for U = 80 m/s with internal pulsed excitation slots at (a) 0.35 and (b) 0.20 diameters upstream of the nozzle exit.

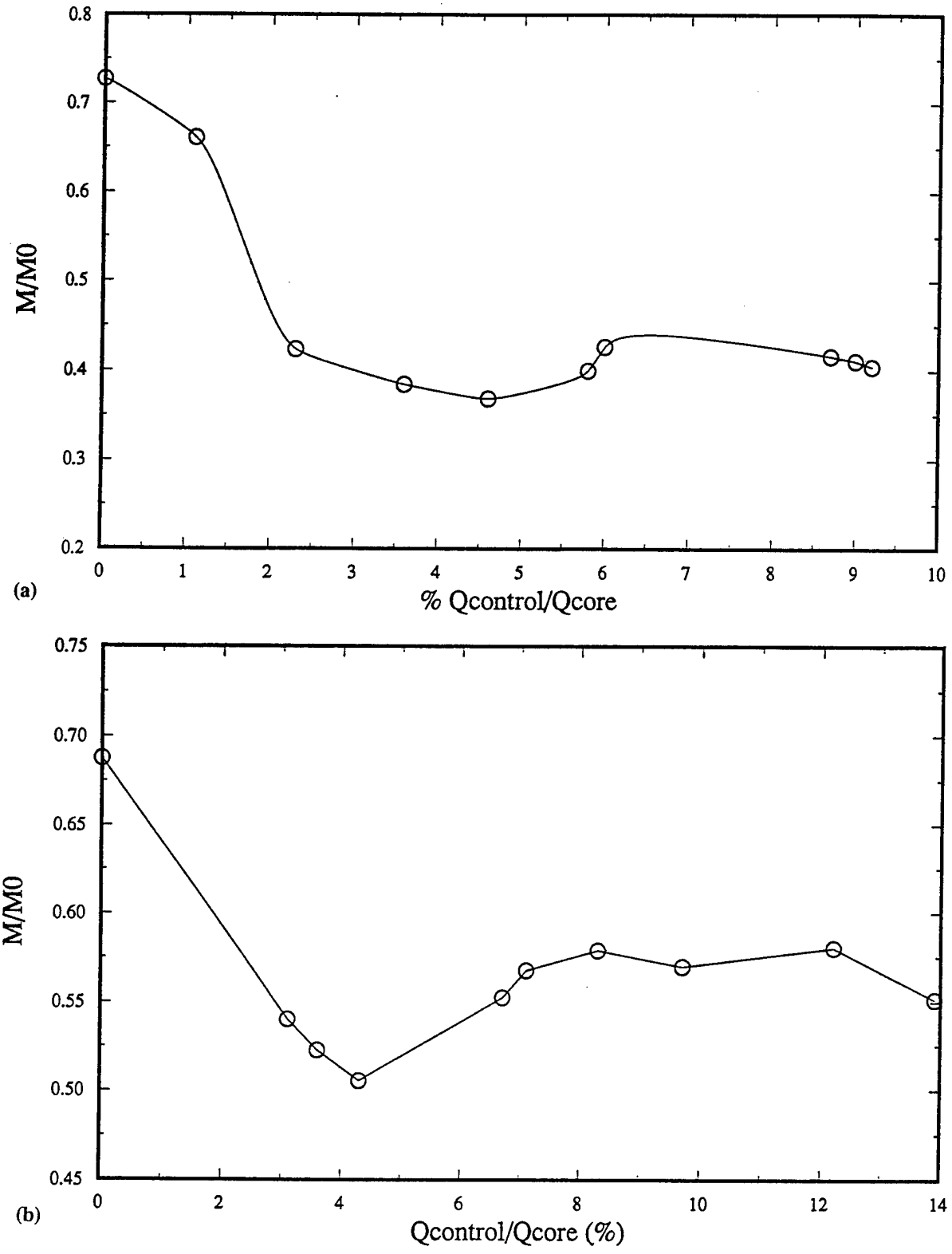

Figure 4.3-6. Centerline velocity at X/D = 10 as a function of excitation amplitude for U = 80 m/s with internal pulsed excitation slots at (a) 0.35 and (b) 0.20 diameters upstream of the nozzle exit. Excitation frequencies corresponding to best mixing in Fig. 4.3-5 are selected for each case: (a) 325 Hz and (b) 475 Hz.

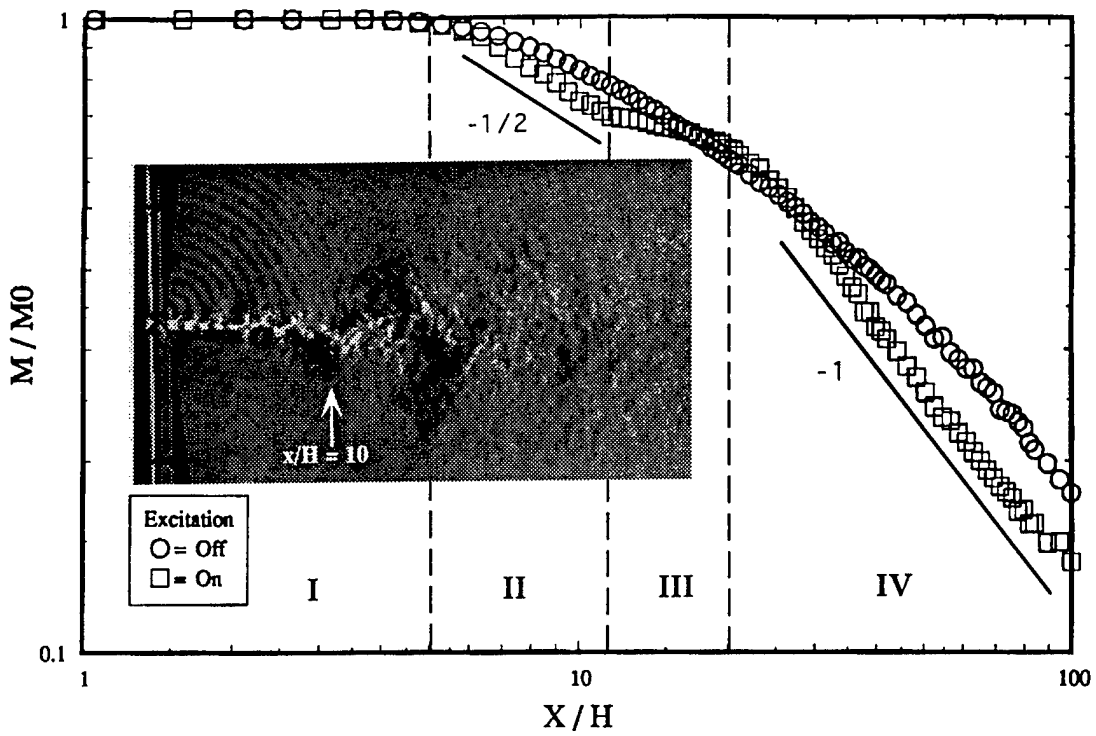

Figure 4.4-1. Comparison of centerline velocity profiles of excited and unexcited 7:1 rectangular jet at M0 = 0.80 and To = 29 C. Excitation frequency and amplitude are 5082 Hz and 122.4 dB, respectively. Schlieren image corresponds to excited 13:1 jet at the same conditions.

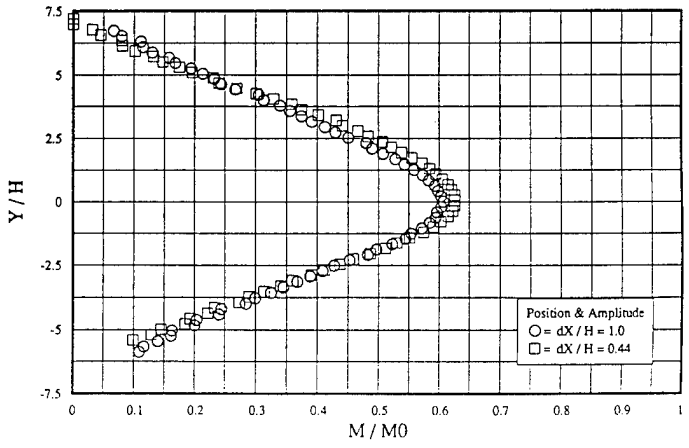

Figure 4.4-2. Sensitivity of velocity profile at X/H = 20 to actuator position. Tip of actuator is located just at the edge of the shear layer at two different streamwise locations measured relative to the nozzle lip.

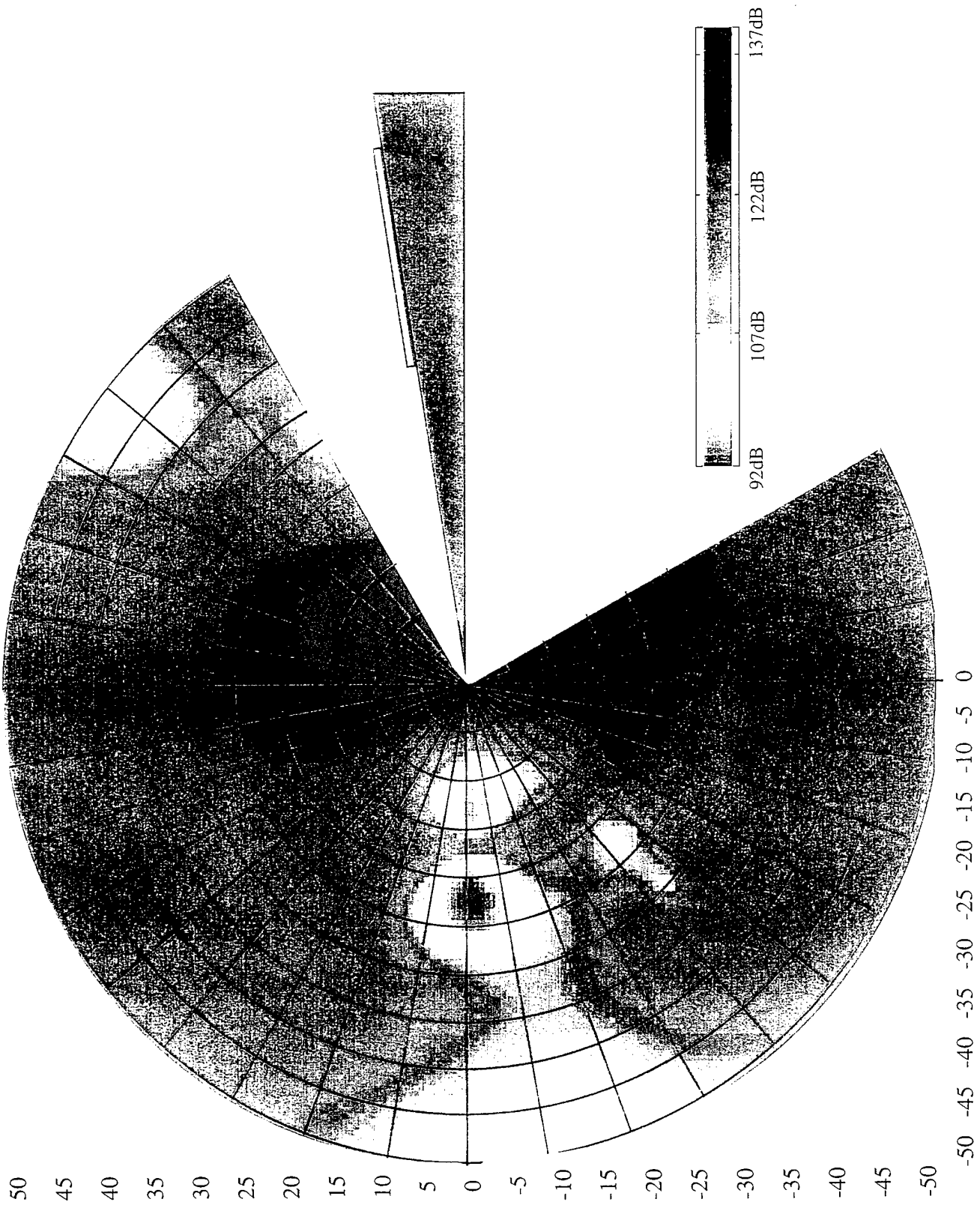

Figure 4.4-3. Polar acoustic amplitude pattern for resonant piezoelectric wedge actuator. All physical dimensions are in mm.

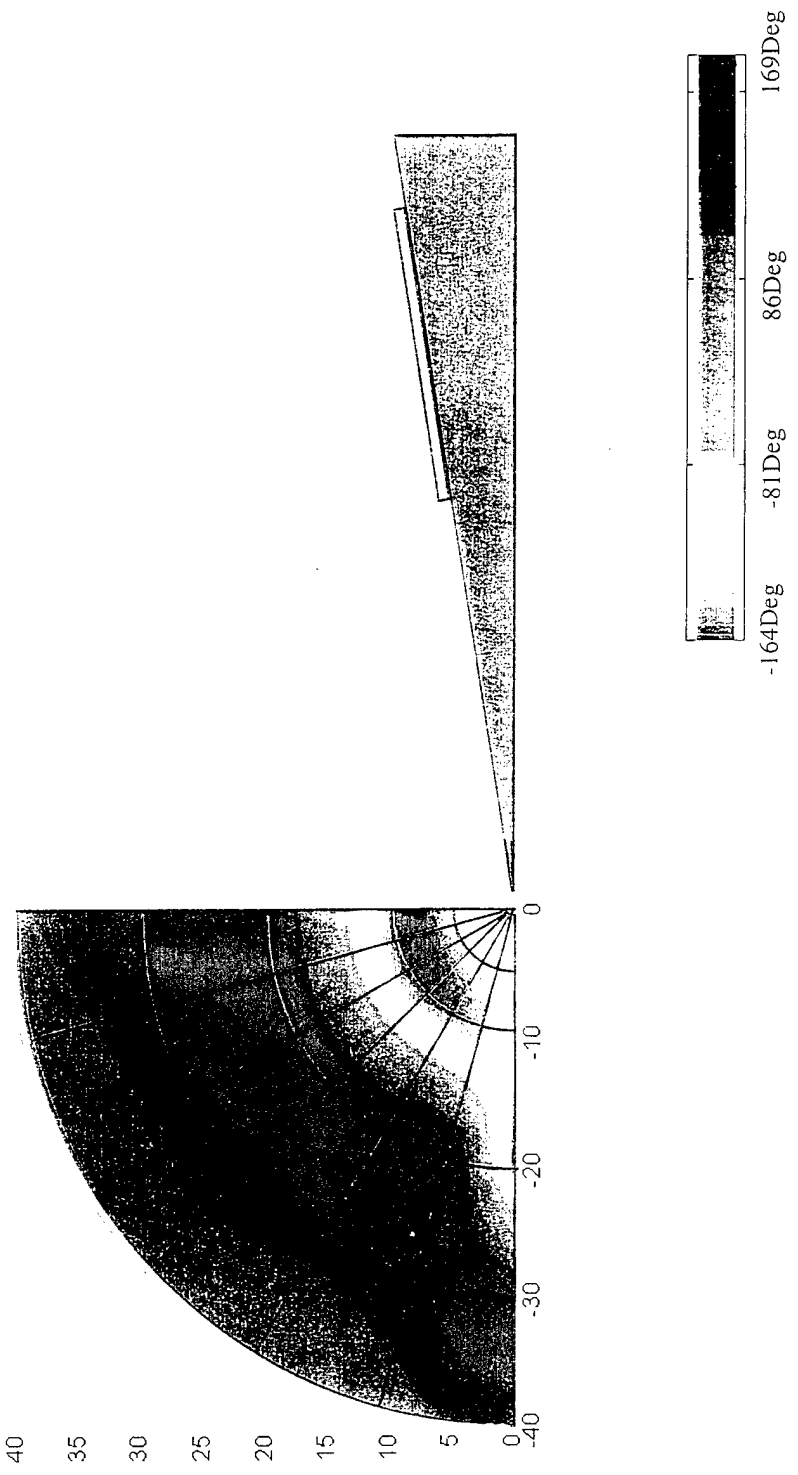

Figure 4.4-4. Polar acoustic phase pattern for resonant piezoelectric wedge actuator. Phase angle is measured relative to reference electrical signal driving piezoelectric elements. All physical dimensions are in mm.

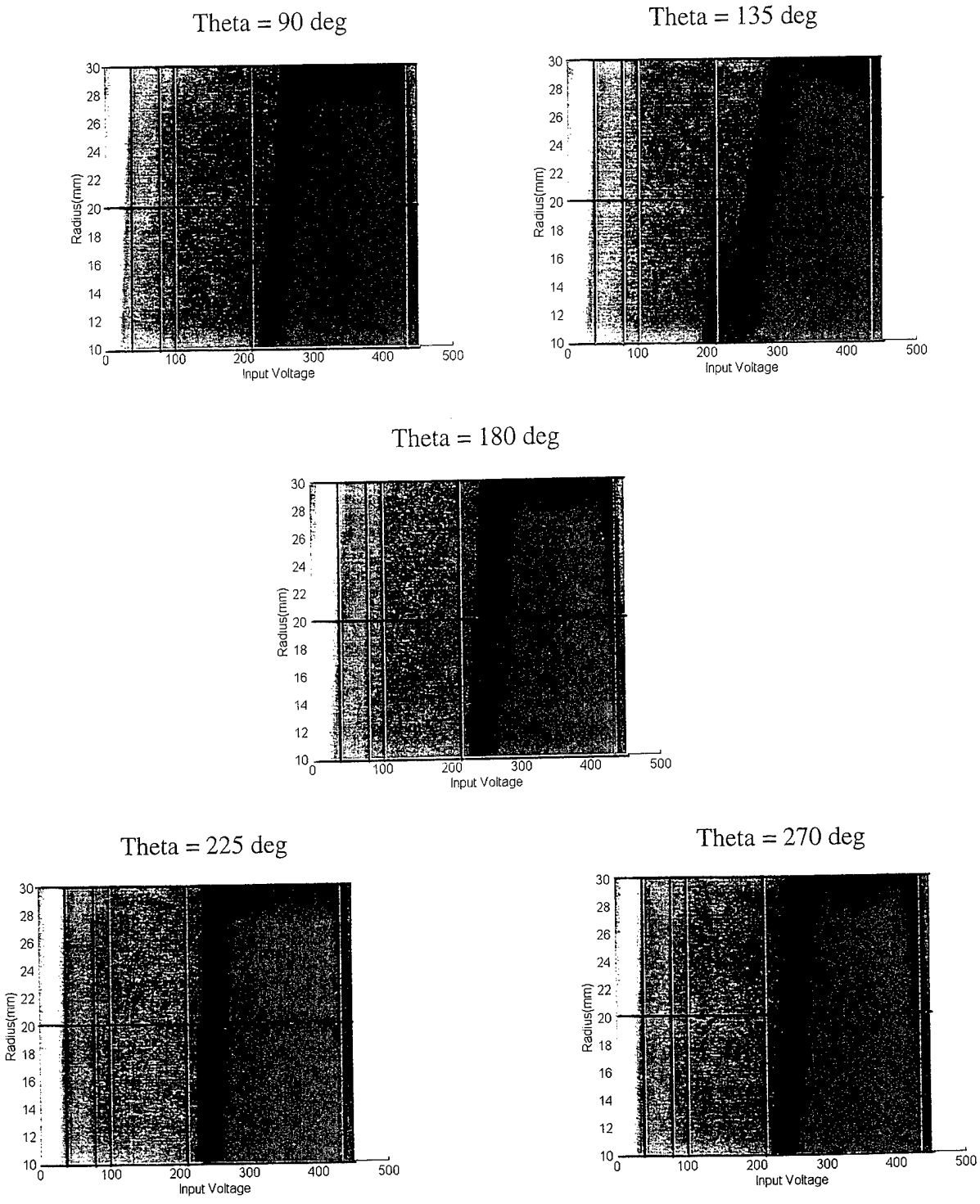

Figure 4.4-5. Acoustic pressure levels as a function of radial position and driving voltage at various polar orientations. All physical dimensions are in mm.

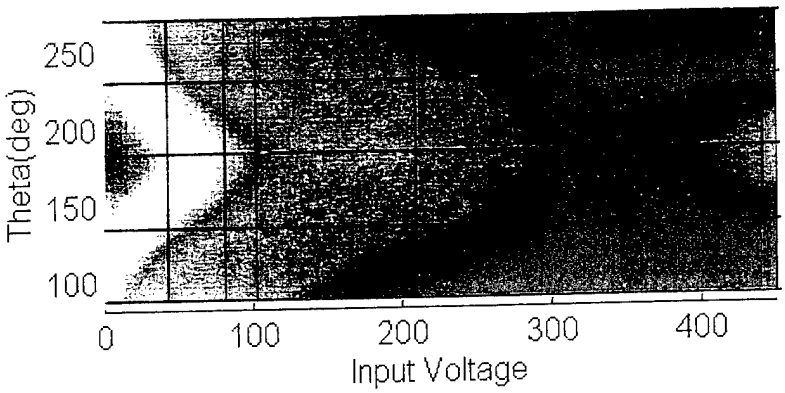

Radius = 10mm

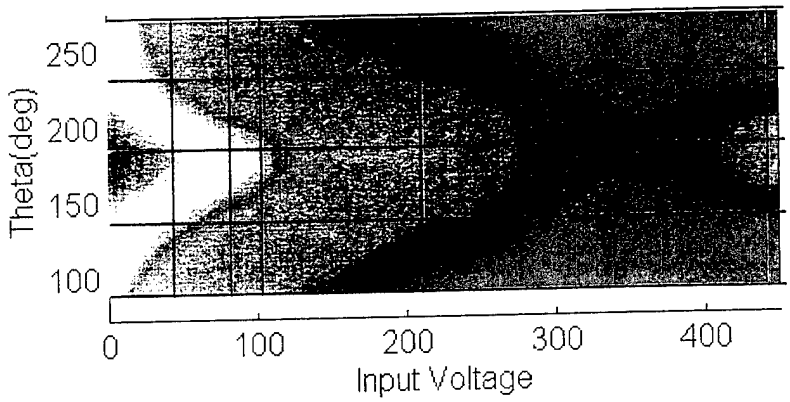

Radius = 20mm

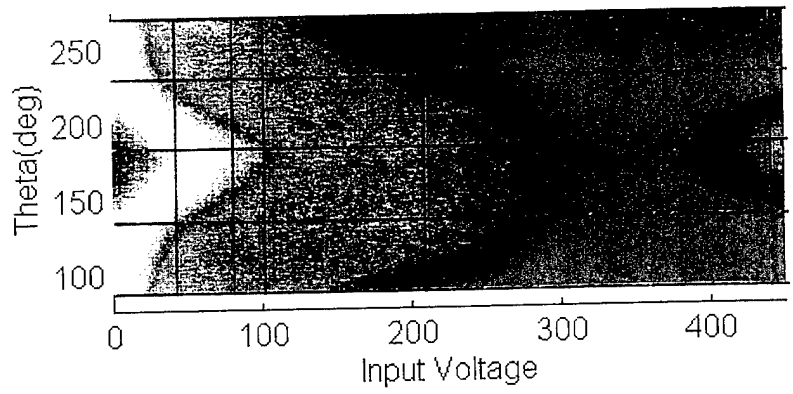

Radius = 30mm

Figure 4.4-6. Acoustic pressure levels as a function of polar orientation and driving voltage at various radial positions. All physical dimensions are in mm.

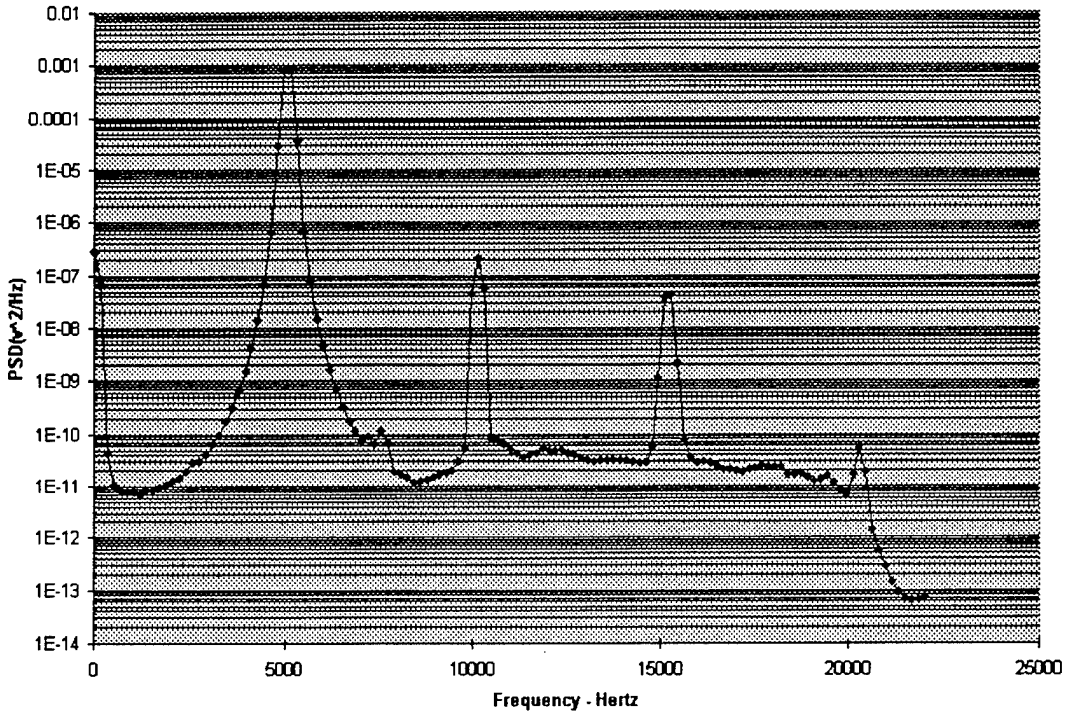

Figure 4.4-7. Power spectrum of acoustic field at a radial distance of 5 mm and a polar angle of 80 degrees.

5. SIMULATION OF FORCED JET RECEPTIVITY

5.1 Flow Visualization of the Nonlinear Computations

A global perspective of the numerical evolution of the forced jet flowfield is provided by examining plots of the vorticity contours. Initially, the jet was forced by both antisymmetric and symmetric forcing (individually tracked). Figure 5.1-1 illustrates a characteristic antisymmetric case. Linear analysis of this time-averaged antisymmetric case produced eigenvalues for the stability behavior that were essentially identical to the linear stability values of the corresponding symmetric case. This should not be surprising since the region of parameter space (shear layer spacing to thickness ratio of nearly 40) we are operating in predicts that the shear layer disturbances are nearly decoupled (between the upper and lower shear layer). We did find that occasionally machine faults, particularly for 32-bit calculations, caused a breakdown in the numerical solutions. This becomes very evident visually in the symmetric cases as the symmetry was broken on occasion by machine faults. Therefore, noting that symmetric and antisymmetric forcing produce nearly identical behavior, all analyses reported will correspond to the symmetric cases as they provided an easy global measure of solution quality by examination of their symmetry.

Figure 5.1-2 through Fig. 5.1-5 provide vorticity contours for four jet flows at Mach 1.5; all cases are for a coflowing stream at Mach 0.15. The coflowing stream is believed to be insignificant as far as the receptivity is concerned, but provides robustness for the numerical solution of the governing equations. Figures 5.1-2 and 5.1-3 both have a characteristic harmonic forcing amplitude of Mach 0.01, but Fig. 5.1.3 has a steady blowing component from the forcing slot of Mach 0.06 instead of 0.01 as in Fig. 5.1-2. Later analysis will show that in a jet of Mach 1.5 this difference has no effect on the receptivity. Figure 5.1-4 is identical to Fig. 5.1-2 except the steady and harmonic blowing amplitudes are increased to Mach 0.05; note that the increases produce a more rapid vortical development. This trend is further reinforced in Fig. 5.1-5 which corresponds to

steady and harmonic amplitudes of Mach 0.25, producing a significantly more rapid vortical development.

Figure 5.1-6 through Fig. 5.1-11 provide vorticity contours for six jet flows at Mach 0.8; all cases are for a coflowing stream at Mach 0.15. Figure 5.1-6 and Fig. 5.1-7 both have a characteristic forcing amplitude of Mach 0.01 and a steady blowing level of 0.01. The dramatic difference is that the case of Fig. 5.1-6 is an isothermal jet/freestream while Fig. 5.1-7 has a jet to freestream temperature ratio of 4.0. The temperature ratio increases the instability growth rate in the jet shear layer, as well as the Reynolds number. Since the increased temperature ratio is achieved by decreasing the freestream Mach number (approximately keeping the convective disturbance velocity constant), there is an effective increase in Reynolds number. The effective increase in Reynolds number is apparent in the development of the thin shear layers. Figures 5.1-8 and 5.1-9 are analogous to Figs. 5.1-6 and 5.1-7 but now the steady blowing level has been increased to Mach 0.06. The vortical structures indicate an increase in receptivity due to the increase in steady blowing. The earlier patterns of temperature ratio effects giving higher instability growth rate and thinner shear layers due to higher Reynolds number are also reinforced. Figure 5.1-10 is analogous to Fig. 5.1-6 with the steady and harmonic forcing both increased by a factor of 5. The increase in forcing amplitude predictably shifts the vortical development upstream. This pattern is reinforced after increasing the steady and harmonic blowing another factor of 5 as illustrated in Fig. 5.1-11. Figure 5.1-11 also captures an early vortex pairing event. Thus, increasing forcing amplitudes from Mach 0.01 to 0.05 and then to 0.25 produces the qualitatively anticipated result of shifting development upstream. Temperature ratio effects are consistent with linear theory and the impact of changing apparent Reynolds number.

Figure 5.1-12 though Fig. 5.1-15 provide vorticity contours for four jet flows at Mach 0.3; all cases are for a coflowing stream at Mach 0.15. Figure 5.1-12 illustrates the symmetrical development of the vorticity contours with steady and harmonic forcing levels of Mach 0.01. Figure 5.1-13 increases the steady blowing component of the

forcing, and the vortical development appears to be accelerated. In Figure 5.1-14 and Fig. 5.1-15, the steady and harmonic forcing levels are both increased by a factor of 5 and 25, respectively (from the reference case of Fig. 5.1-12). The visualization of these last two cases leaves no doubt about the accelerated vortical development of the flowfield with increased forcing amplitude. In the coming discussion we will quantify the receptivity behavior for most of the 15 figures discussed in this section.

5.2 Flow Solution Generation and Analysis

Our general purpose flow solver NASTD was used to generate the nonlinear flow solutions that provide a base flow for the linear stability theory, as well as the nonlinear solution evolution. NASTD is an Euler and Navier-Stokes solver developed at Boeing–Phantom Works and in production use. NASTD operates in two or three dimensions with structured (patched and overlapping) and unstructured grids. Any valid grid can be utilized; NASTD places no restrictions on the point or slope discontinuities at zone interfaces. A mature zone coupling technique, in production since 1985, ensures continuity of the solution across zone boundaries. NASTD has a library of boundary condition routines available on a point-by-point basis.

NASTD has been used for flows from nearly incompressible speeds ($M<0.05$) to hypersonic velocities. Turbulence can be modeled by a variety of algebraic, one and two equation turbulence models. The default scheme for most NASTD applications is the Spalart-Allmaras one equation model which provides reasonable accuracy for attached and separated boundary layers as well as shear layers. A low Reynolds number form of the Menter two equation model is the preferred higher order model. The present effort is based strictly on laminar flow calculations.

NASTD incorporates a number of user-selectable (by zone) solution algorithms. The default time integration scheme is a first order, approximately factored implicit scheme. For inviscid flows (or, under the thin layer approximation, for directions with no viscous terms) the implicit operator is diagonalized, providing a significant speed-up. Explicit

Runge-Kutta options of up to third order are also available for time-accurate flowfields. For steady-state flows, variable time steps based on local eigenvalues are used to speed convergence. Grid sequencing is available to speed convergence on large grids.

The default explicit spatial operator is a second order Roe flux difference split scheme. The standard upwind operator has been replaced by a physical space scheme which retains the upwind-biased-scheme stability properties with reduced numerical dissipation. Optionally, the scheme may be switched to various first through fifth order schemes and total variation diminishing (TVD) limiters may be activated. Other available schemes include standard second order central differencing with added second and fourth order dissipation. The present analysis is based on the fifth order spatial operator and the third order Runge-Kutta time integration.

NASTD has been written in standard FORTRAN-77 and ports easily to most computer platforms. NASTD is currently operational on Cray, Convex, VAX, Silicon Graphics, Hewlett Packard, Intel and IBM platforms.

5.2.1 Grid Generation

Various aspects of the grid generation process are critical to obtaining highly accurate, clean CFD solutions. In order to eliminate errors due to boundary approximations, single zone grids with no symmetry plane are used. Running on a full geometry also allowed us to determine breakdowns in the solution by using symmetric forcing and watching for the development of asymmetries in the flowfield. The outer normal boundaries were angled to reduce noise from uncertainty in the incoming versus outgoing characteristic information that occurs in solutions that have boundaries tangent to the mean flow direction. Axial grid spacing at the nozzle exit was identical to the normal spacing and equal to the plate thickness, 0.05". The nozzle lip thickness and grid spacing near the exit are very small compared to the instability wavelength. In particular, the instability wavelengths are all within 20% of 20", making the nozzle lip thickness and grid spacings 1/400 of an instability wavelength. Grid stretching was limited to 3% to limit numerically generated dispersion. An attempt was made to appropriately scale each of the cases, to

allow the use of the same grid. However, separate upstream grids were generated for cases with a supersonic jet Mach number. The grid used for subsonic jet Mach numbers is shown in Figure 5.2-1. A converging/diverging nozzle was simply added upstream of this grid for cases with a supersonic jet Mach. The jet velocity and forcing frequency were selected such that the wavelength of the forced disturbance varied by less than 20% for each of the cases run. The number of grids points per wavelength varied from 400 at the nozzle trailing edge to approximately 21 at the axial station farthest downstream.

5.2.2 Methodology

The two-stream flow with harmonic blowing was modeled using plates of length 20" and thickness 0.05" as shown in Figure 5.2-1. Freestream characteristic conditions were specified for the outer flow. An arbitrary inflow boundary at the jet conditions was specified at the inflow between the plates. Harmonically forced disturbances are introduced 1" upstream from the exit of the nozzle on the nozzle interior over a slot width of 0.15". The harmonically forced disturbance has a steady state offset velocity that has been varied from equal to the harmonic amplitude to 6 times larger than the harmonic amplitude.

Throughout the course of this study, various process improvements were made to ensure high fidelity in our CFD solutions. In order to diminish spurious reflections at boundaries, a boundary damping scheme was used at all four boundaries. This amounts to a numerical viscosity that is linearly varied from a strong dissipation at the boundary to no effect three disturbance wavelengths from the boundary. After evaluation of several computational schemes, we modified our code to run a highly accurate 5th-order Roe scheme. A sensitivity to the platform precision was discovered. We have run on 64-bit machines whenever possible. However, due to hardware availability, several cases were run on 32-bit machines. Convergence criteria used to attain a stationary state conditions were based on the change in delta omega at various axial stations. A stationary state in the solution was assumed when delta omega varied by less than 0.1% from one

period of forcing to the next at each of the axial stations where linear stability analysis was performed. As indicated in Table 5.2-1, not all cases attained a stationary state.

5.2.3 Receptivity Based on Linear and Nonlinear Computation

Upon achieving a stationary state in the nonlinear CFD solutions, a time history file was generated along a line extending from the plate trailing edge and along vertical lines at various axial stations. The TIMPLT code, described below, was used to process the data from these time history files. The harmonic disturbance amplitude distribution downstream from the nozzle lip was examined. The axial distribution of the harmonic disturbance amplitude helps select appropriate axial stations for performing the linear stability analyses using DynaFlow's LISA code. The harmonically forced disturbance that exits from the slot in the nozzle will contain a collection of eigenmode and possibly continuous spectrum modes. After convecting some distance downstream the dominant discrete eigenmode of the shear layer at the forced frequency will contain almost all of the disturbance energy.

However, in the region near the nozzle disturbances other than the dominant eigenmode can be significant. The results from LISA were used to generate nondimensional growth rate curves. The curves of harmonic disturbance amplitude were used to determine when the dominant eigenmode contained most of the energy and to estimate growth rates of the dominant forced disturbance in the region near the nozzle lip where the nonlinear disturbance contains information not yet dominated by the dominant eigenmode.

The computed growth rates from the linear stability analysis and the nonlinear computation of the harmonic amplitudes are used to calculate a receptivity coefficient. Two definitions for the receptivity coefficient have been examined. The first is simply the ratio of the magnitude of the disturbance fluctuation at the nozzle lip to the amplitude of the fluctuating component of the forcing. The second definition of receptivity coefficient is due to Kerschen (1996). Kerschen defined the receptivity coefficient as the ratio of the response disturbance amplitude at the receptivity site (the trailing edge in this

case) to the forcing source strength (disturbance velocity times the slot width) times the forcing frequency divided by the jet velocity. Kerschen (1996) examined cases where the flight speed or freestream velocity were zero. We correct for a finite flight velocity by using Kerschen's original definition but replacing the jet velocity by twice the convective speed of the forced vortical disturbance. The resulting expressions match for the case of zero flight speed.

Figures 5.2-2 through 5.2-6 show examples of analytical linear predictions of the receptivity coefficient (Kerschen, 1996) and receptivity coefficients determined by nonlinear computation from the present AFOSR contract effort. We begin by considering a jet Mach number of 0.8. Figure 5.2-2 illustrates the receptivity coefficient analytically predicted for the excitation location from near the nozzle lip to 5 nondimensional distances upstream (the upstream location is nondimensionalized by the jet velocity and angular frequency) and by nonlinear computation for the excitation near the nozzle lip. Note that the nonlinear computation with the smallest amplitude forcing is essentially identical to the analytical prediction. This match between linear theory and low amplitude is remarkable in view of the complexity of the process. The computation also predicts a decreasing receptivity coefficient with increasing forcing amplitude. These results suggest that the lowest amplitude forcing is below the threshold of nonlinear response, but that larger forcing amplitudes do exhibit nonlinearity. Note also that the nonlinear computation represented by the black circle shows that constant blowing in addition to harmonic forcing can increase the receptivity coefficient by 40%.

Figure 5.2-3 is analogous to 5.2-2, but the Mach number is now 1.5. In this supersonic case the linear theory underpredicts the low amplitude nonlinear computation but the computational cases still span the linear prediction. Note that the two lowest amplitude forcing computations give the same receptivity coefficient implying linearity in the response. The increase in the threshold of nonlinearity with the supersonic jet is logical and somewhat reassuring. The discrepancy between the analytical prediction of linear theory and the nonlinear computation is believed to be due to compressibility

considerations that differ between the nonlinear computation and the linear theory, though the presence of a Mach 0.15 freestream might potentially have some impact.

Figure 5.2-4 shows that increasing the Mach number from 0.8 to 1.5 reduces the receptivity coefficient by roughly a factor of 2. Figure 5.2-5 shows that increasing the temperature ratio between the jet and the freestream from 1.0 to 4.0 reduces the receptivity coefficient between 25% and 50%. In Fig. 5.2-6 the effect of steady blowing is seen to increase the receptivity coefficient 40% for a Mach 0.8 jet but have no effect (for these modest blowing levels) on the Mach 1.5 jet. The reason for the last result is likely explained by a complete separation (no reattachment) of the nozzle for the Mach 0.8 case thus increasing the receptivity coefficient. The blowing level is likely insufficient in the Mach 1.5 case, and the separation is probably small and local, thus not changing the receptivity coefficient.

5.3 Raw Data Processing

Figure 5.3.1 is an example of the comparison between the LISA linear theory prediction of the instability growth rate and the processed nonlinear computational result. The red curve is produce by averaging the local computational result over 1/2 of a forced wavelength. While the prediction of linear theory and the nonlinear computation aren't identical, it is apparent that after approximately 1/4 of a wavelength the nonlinear and linear growth rates are roughly the same. Plots similar to this were examined for all cases. Some cases show closer agreement while others agree less closely.

Figure 5.3.2 is an example of the harmonically decomposed disturbance levels (of the velocity perturbation perpendicular to the jet flow) as a function of distance downstream from the nozzle lip (in the streamwise direction). This reference case shows the clear dominance of the forced frequency as well as a nearly exponential growth for a considerable distance before saturating. Some of the other cases show more significant harmonic amplitudes, but this plot provides a clue as to the nature of the flow and the processing approach.

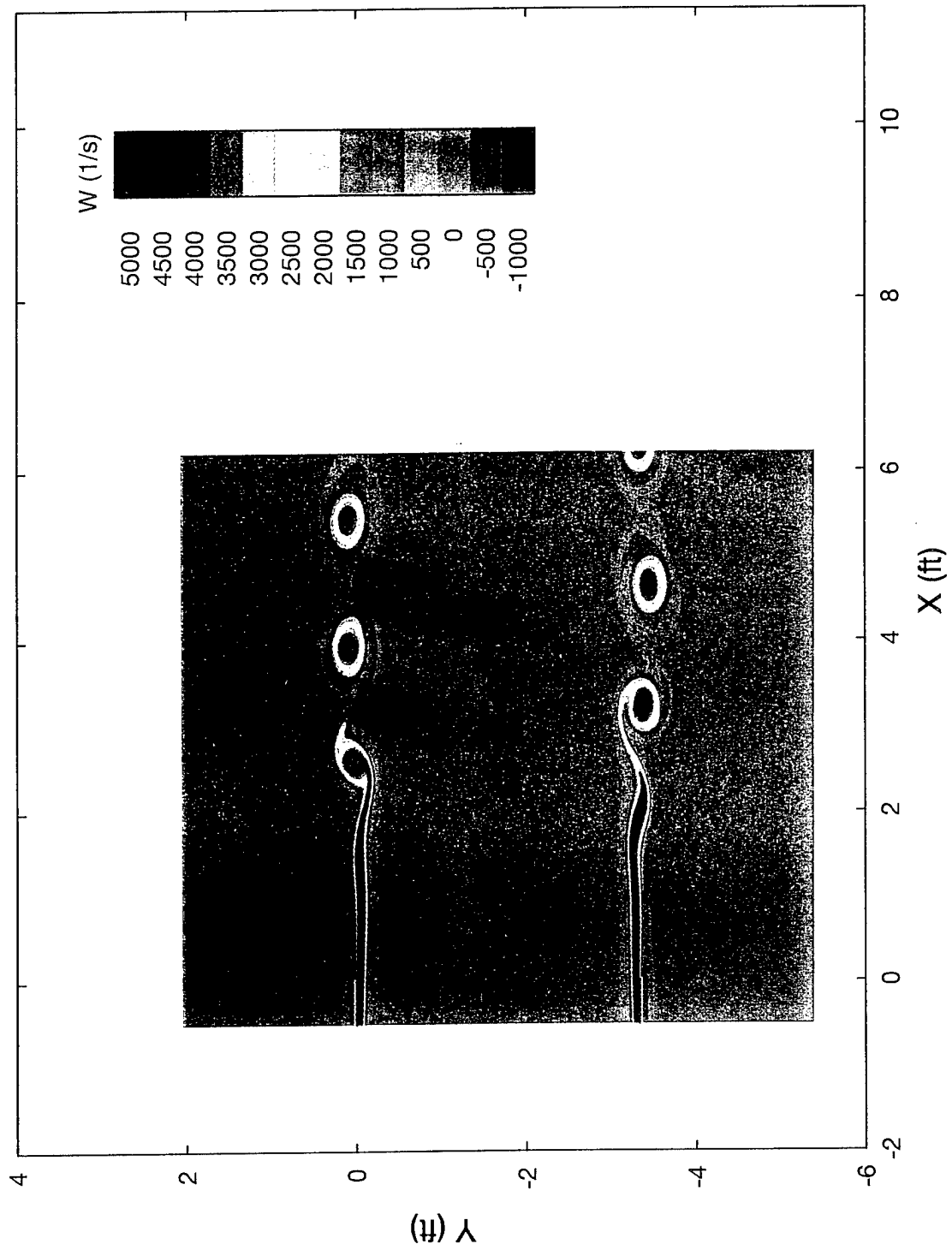

Figure 5.1-1. Vorticity Magnitude for Antisymmetric Isothermal Case, Minf=0.8, Steady Blowing Amplitude=0.05, Harmonic Forcing Amplitude=0.05.

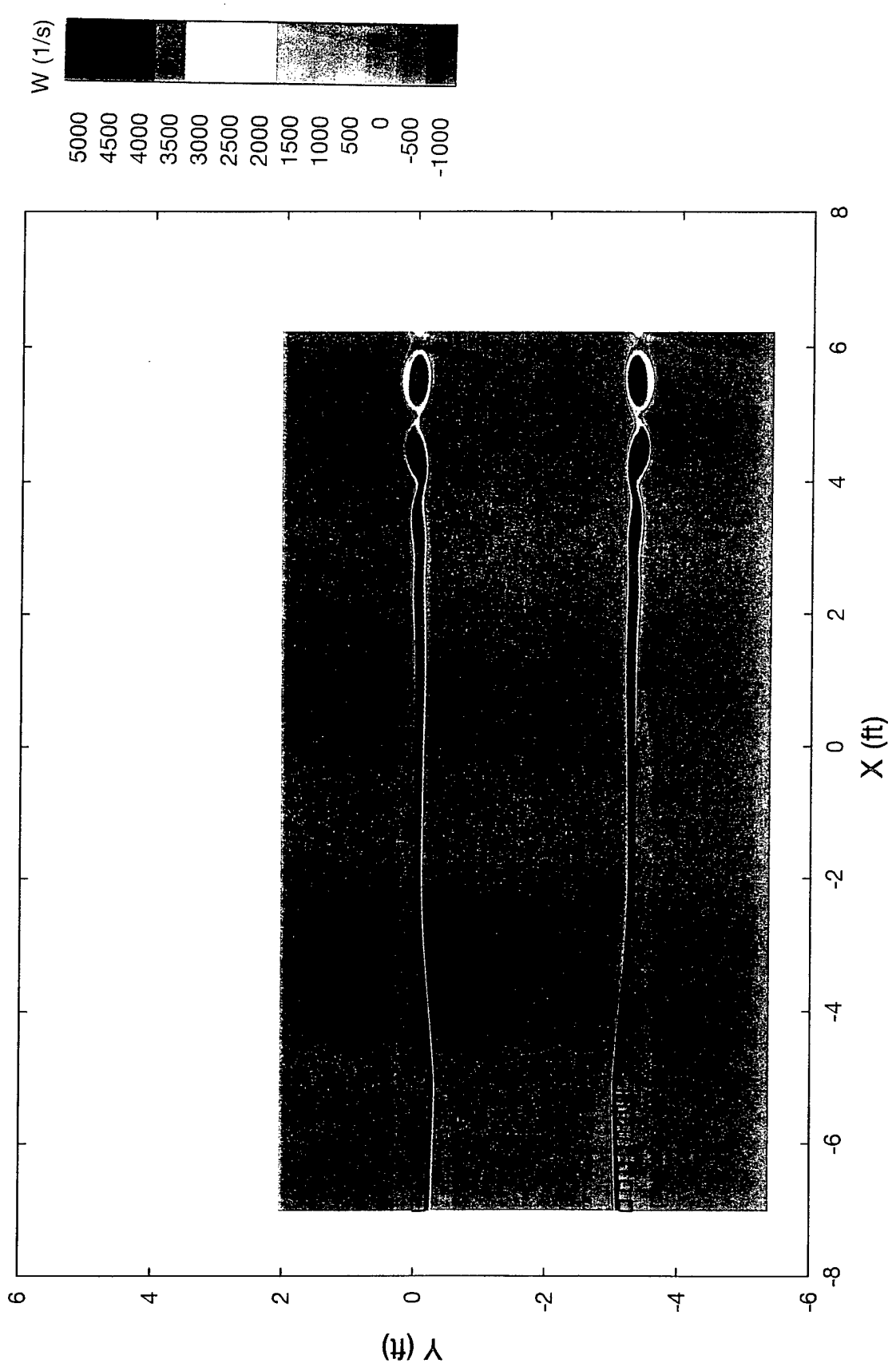

Figure 5.1-2. Vorticity Magnitude for Symmetric Isothermal Case, Minf=1.5, Steady Blowing Amplitude=0.01, Harmonic Forcing Amplitude=0.01.

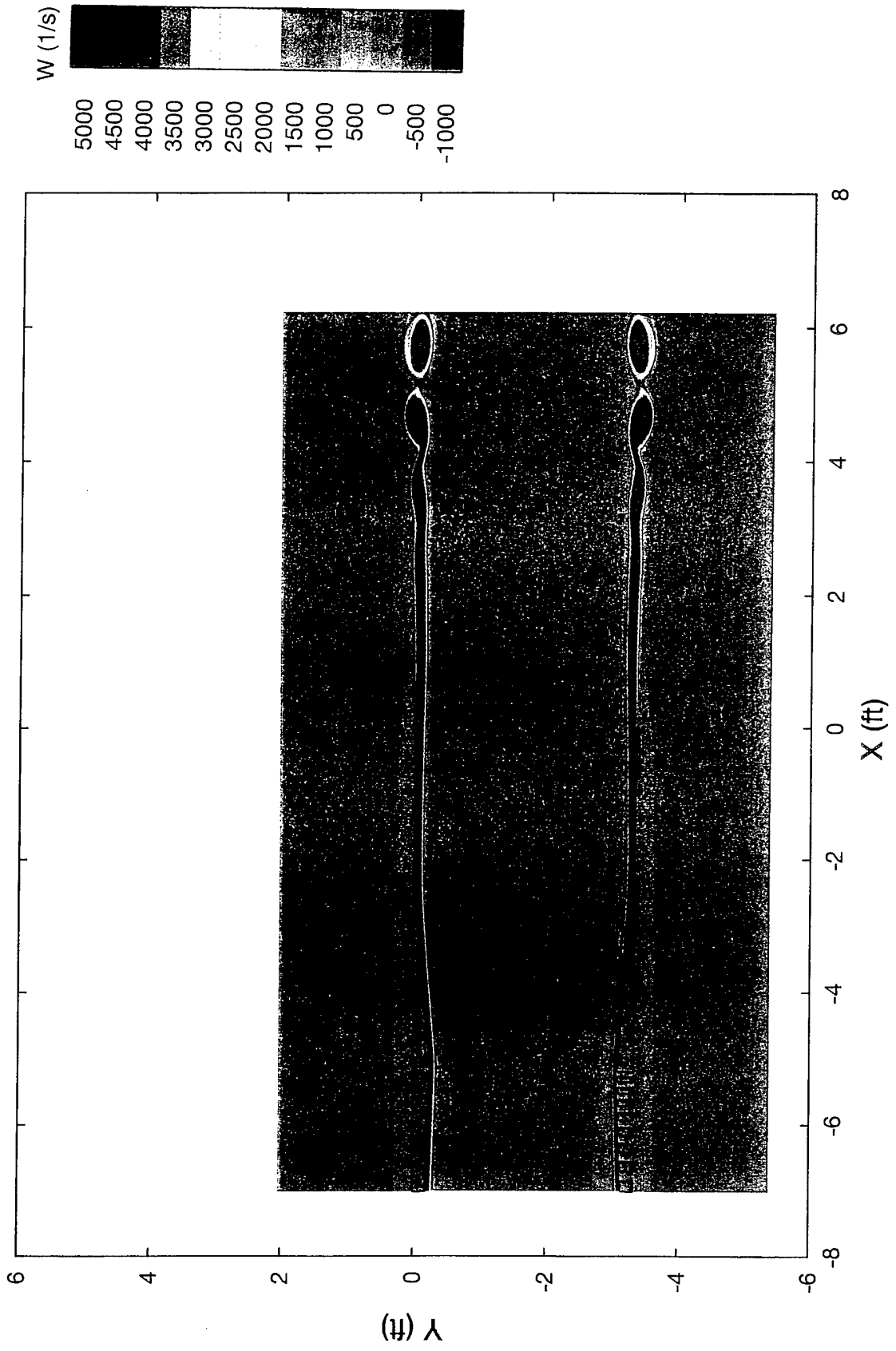

Figure 5.1-3. Vorticity Magnitude for Symmetric Isothermal Case, Minf=1.5, Steady Blowing Amplitude=0.06, Harmonic Forcing Amplitude=0.01.

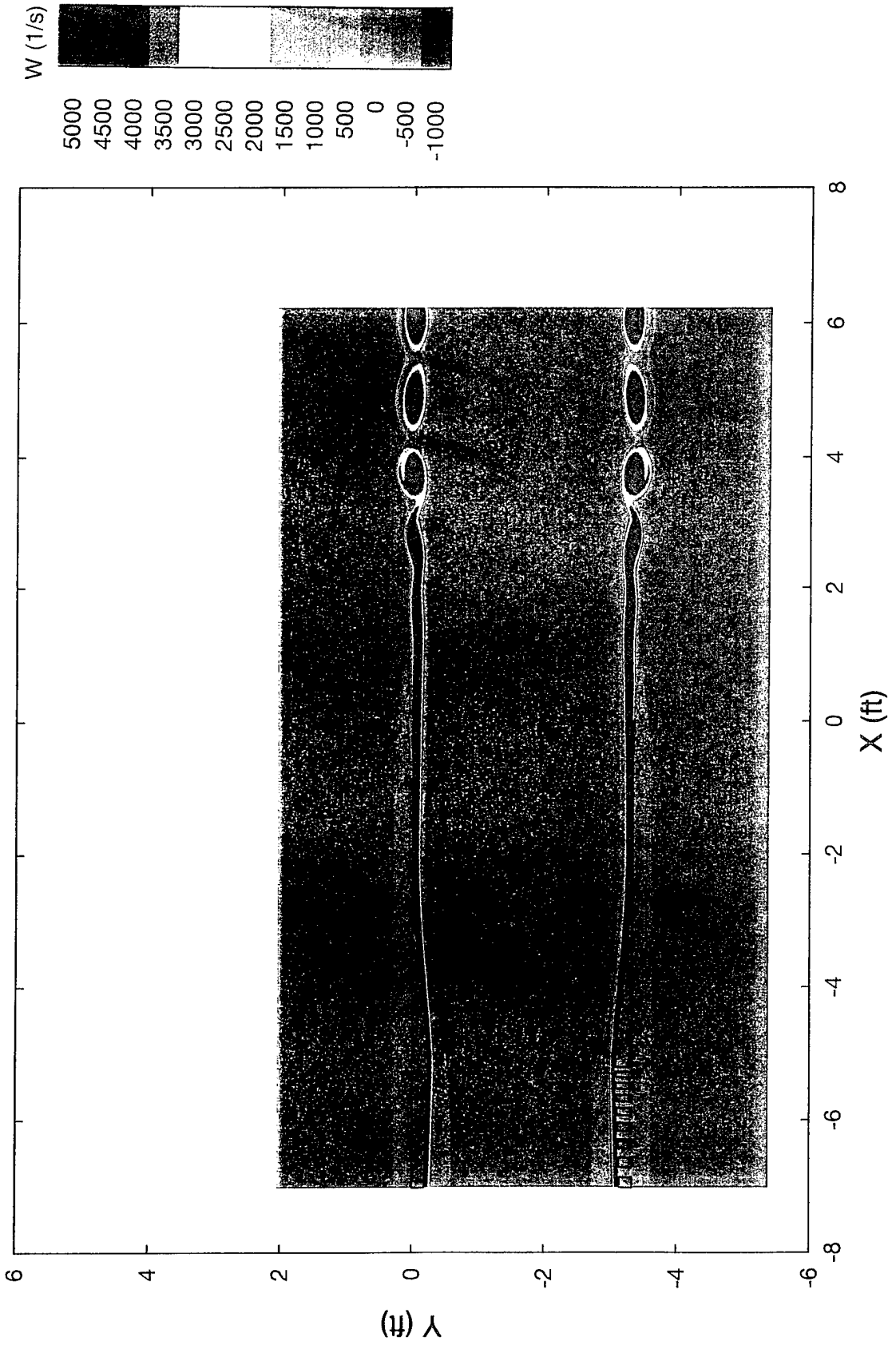

Figure 5.1-4. Vorticity Magnitude for Symmetric Isothermal Case, Minf=1.5, Steady Blowing Amplitude=0.05, Harmonic Forcing Amplitude=0.05.

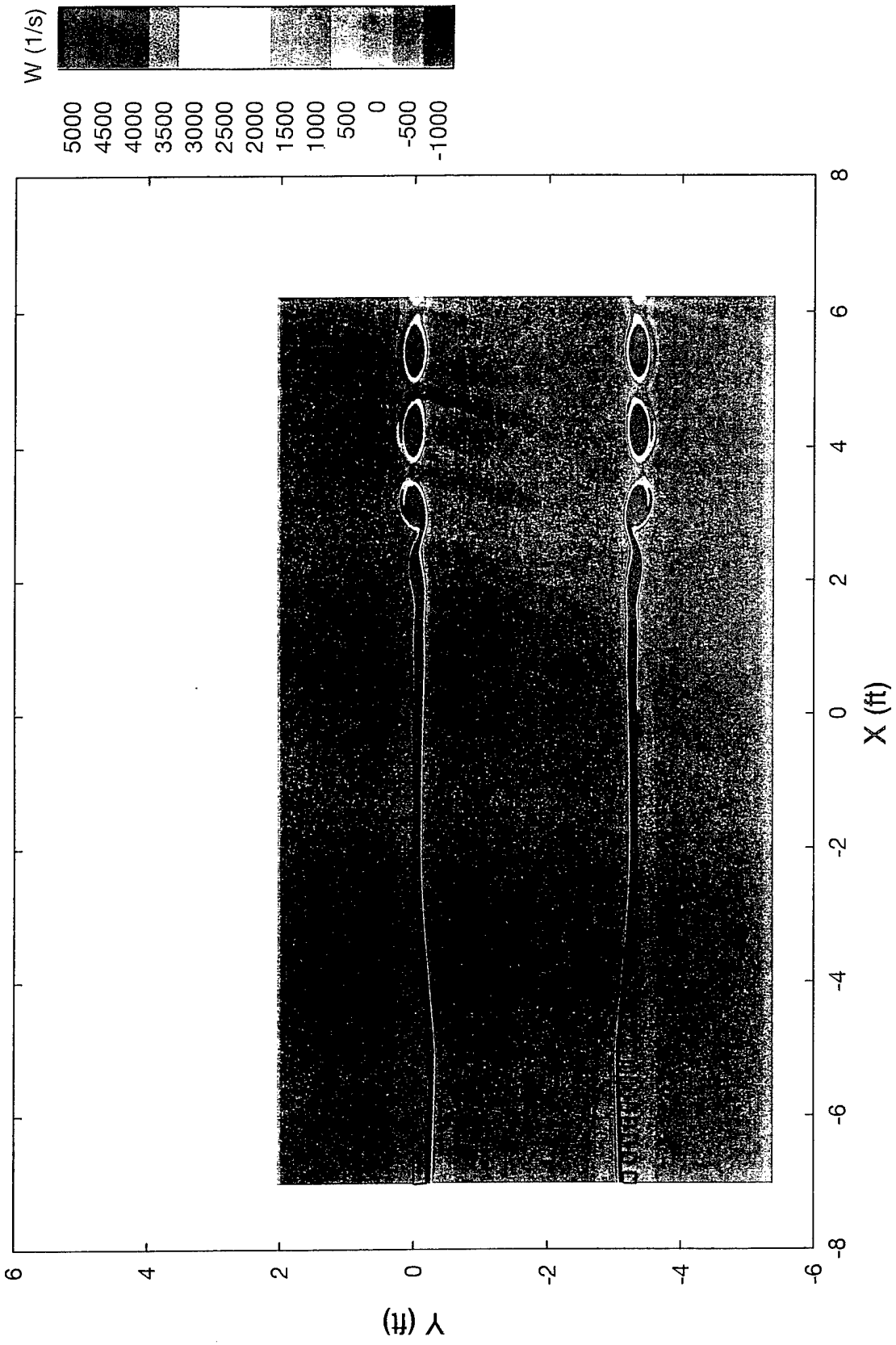

Figure 5.1-5. Vorticity Magnitude for Symmetric Isothermal Case, Minf=1.5, Steady Blowing Amplitude=0.25, Harmonic Forcing Amplitude=0.25.

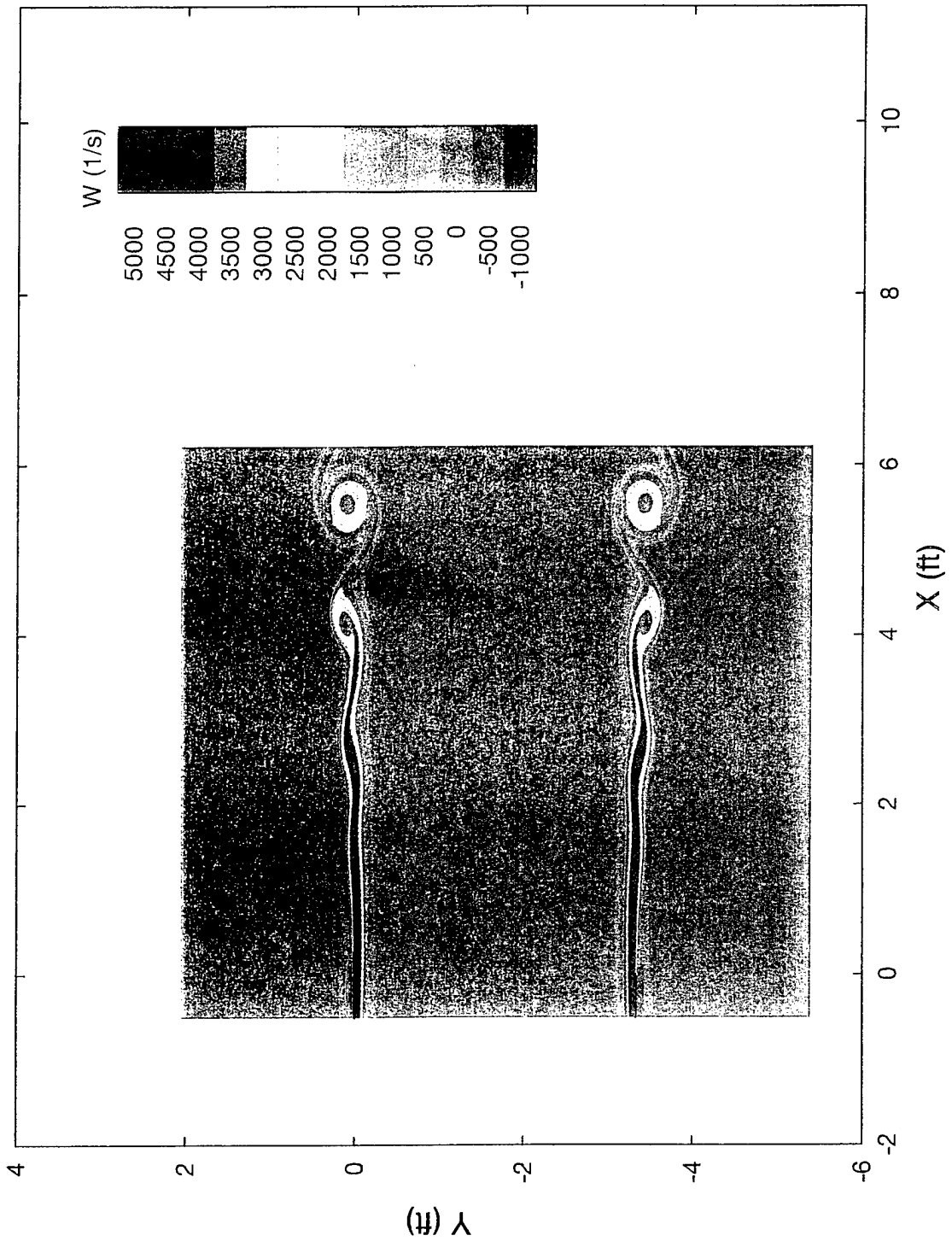

Figure 5.1-6. Vorticity Magnitude for Symmetric Isothermal Case, Minf=0.8, Steady Blowing Amplitude=0.01, Harmonic Forcing Amplitude=0.01.

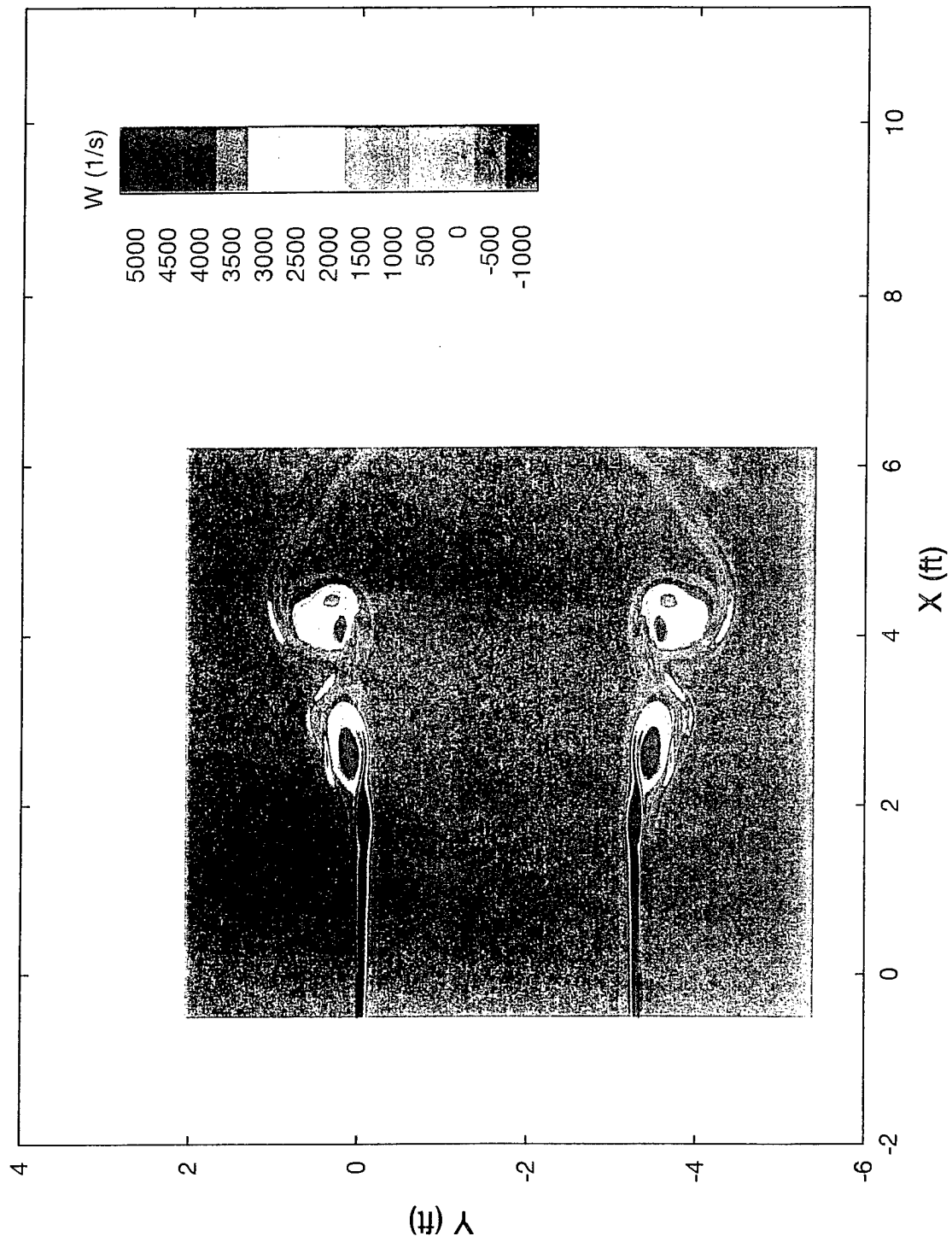

Figure 5.1-7. Vorticity Magnitude for Symmetric Case, Minf=0.8, Tj/Tinf=4.0, Steady Blowing Amplitude=0.01, Harmonic Forcing Amplitude=0.01.

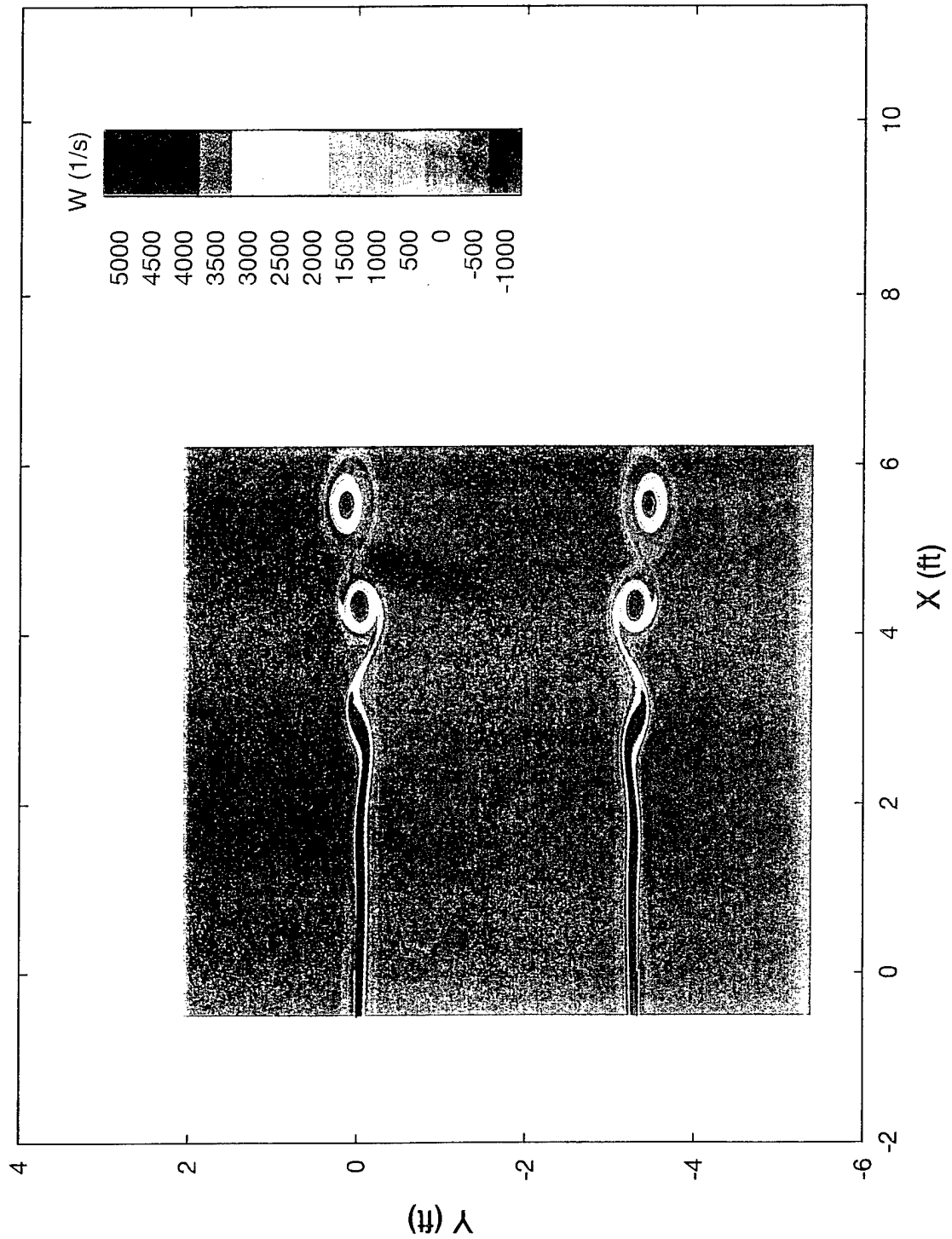

Figure 5.1-8. Vorticity Magnitude for Symmetric Isothermal Case, Minf=0.8, Steady Blowing Amplitude=0.06, Harmonic Forcing Amplitude=0.01.

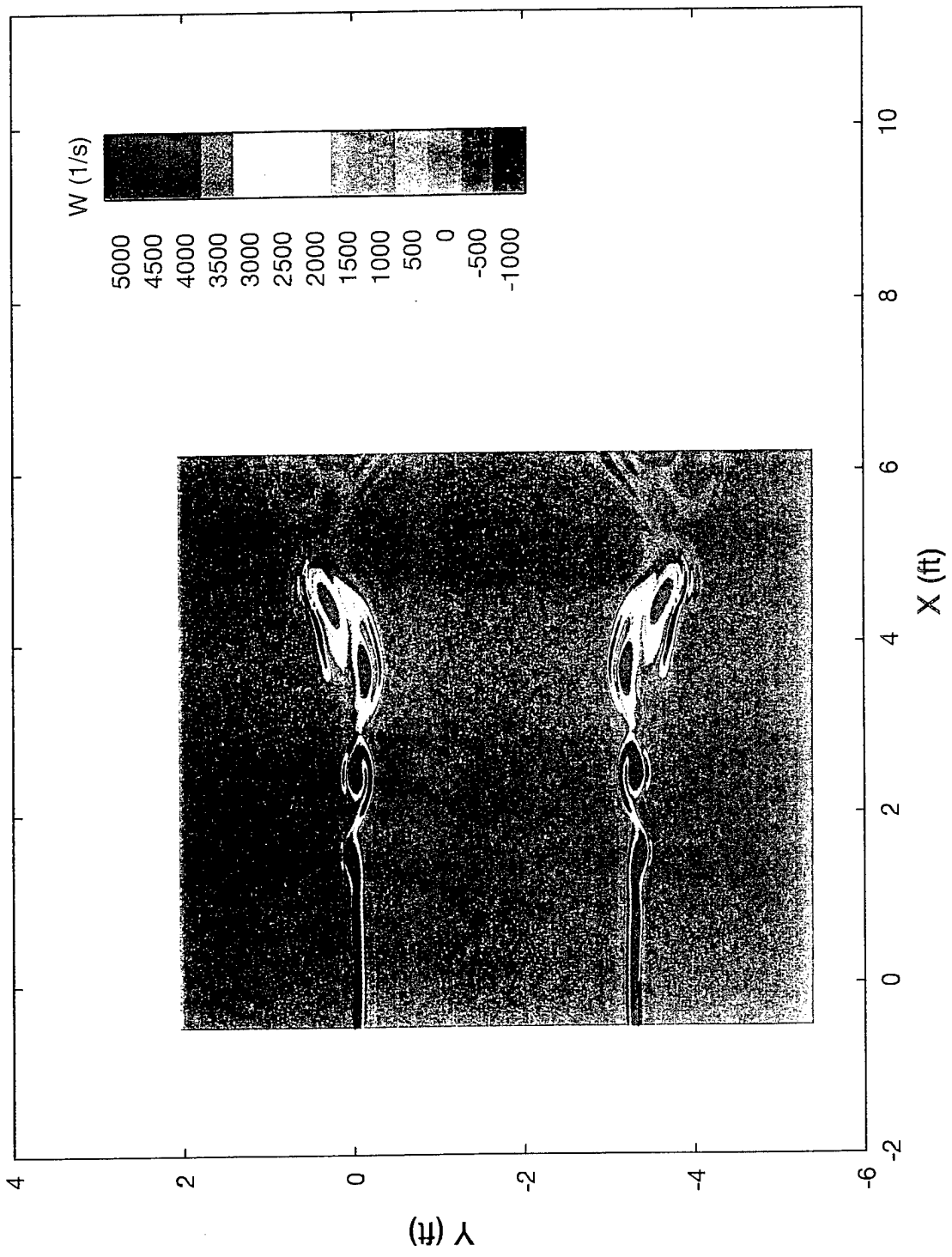

Figure 5.1-9. Vorticity Magnitude for Symmetric Case, Minf=0.8, Tj/Tinf=4.0, Steady Blowing Amplitude=0.06, Harmonic Forcing Amplitude=0.01.

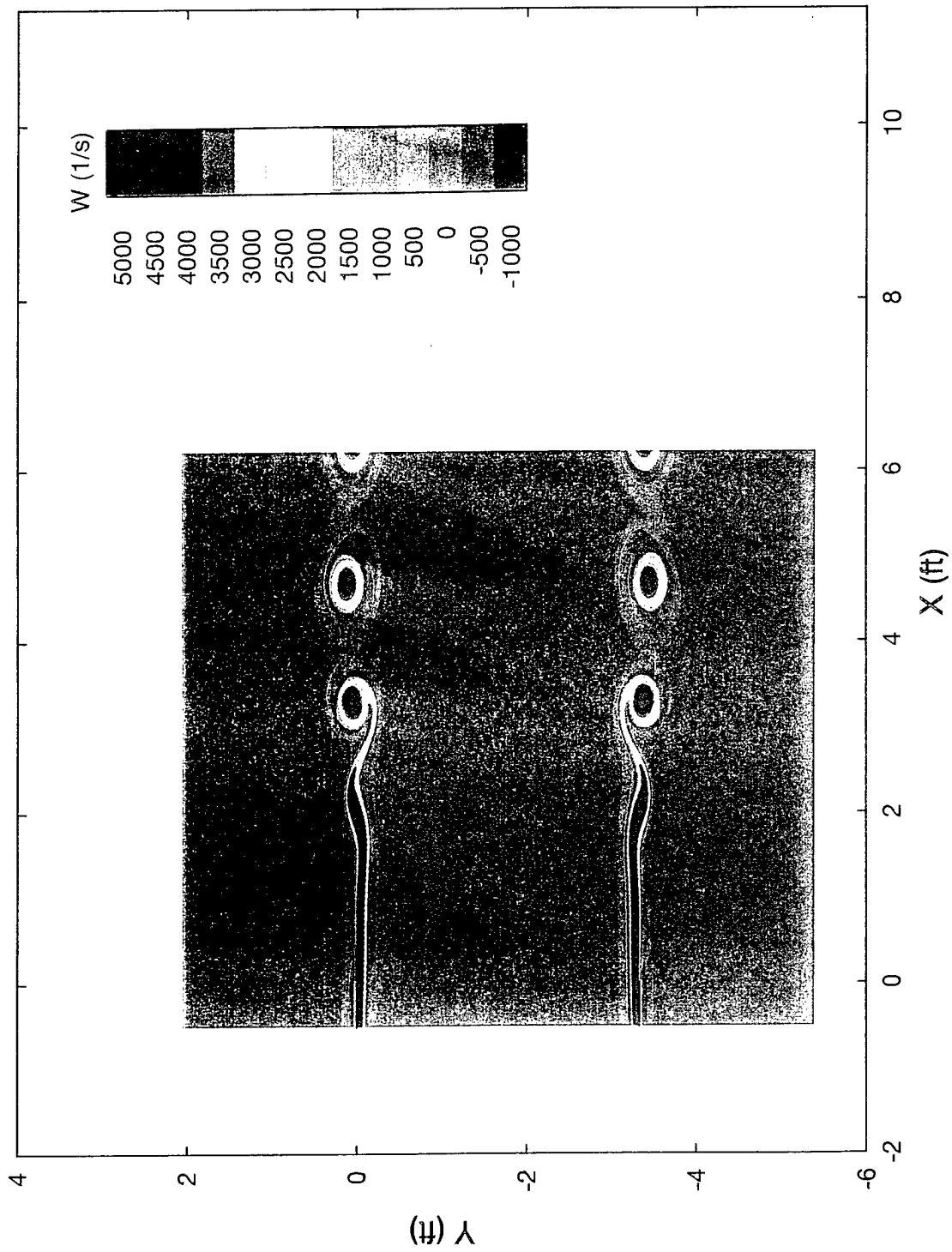

Figure 5.1-10. Vorticity Magnitude for Symmetric Isothermal Case, Minf=0.8, Steady Blowing Amplitude=0.05, Harmonic Forcing Amplitude=0.05.

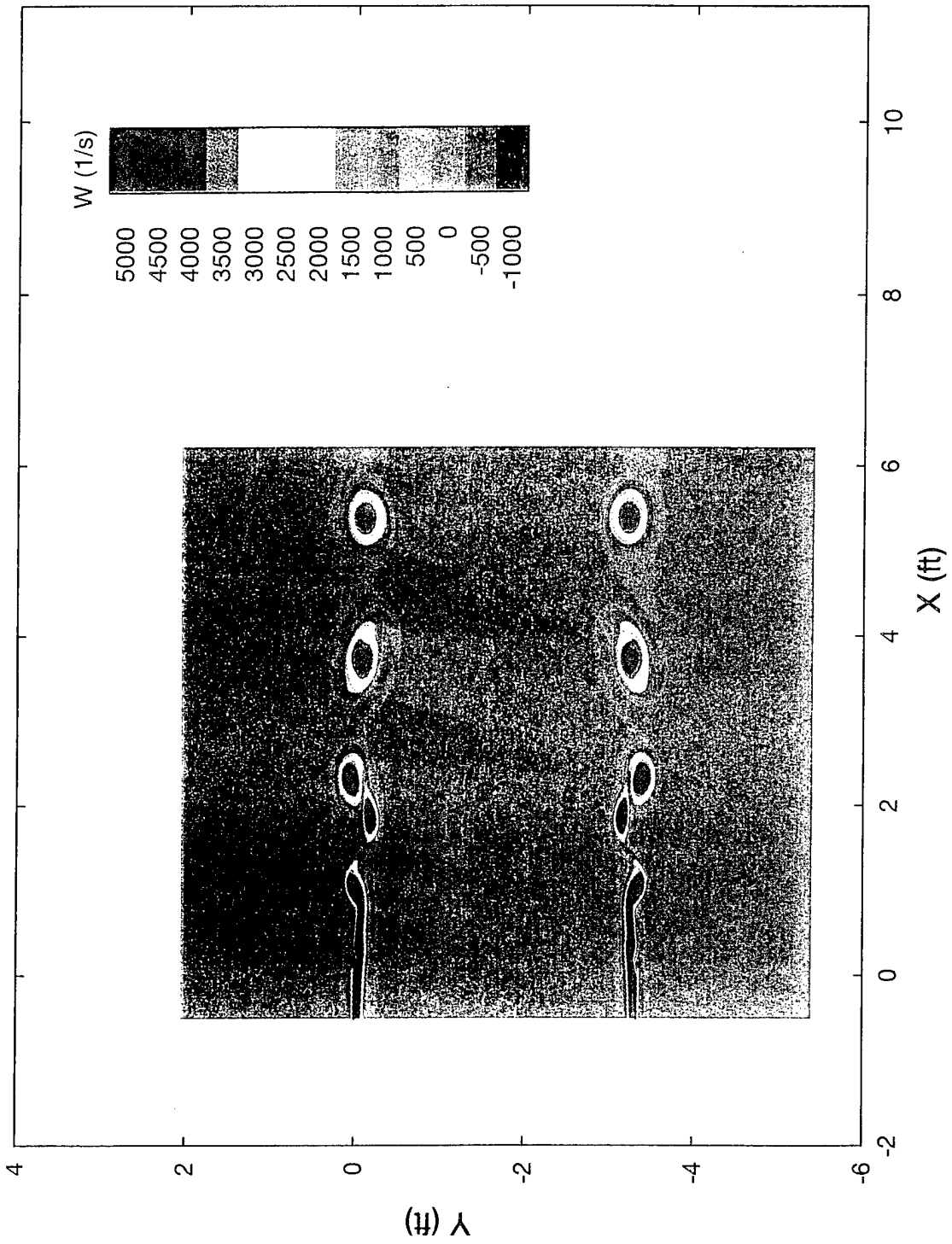

Figure 5.1-11. Vorticity Magnitude for Symmetric Isothermal Case, Minf=0.8, Steady Blowing Amplitude=0.25, Harmonic Forcing Amplitude=0.25.

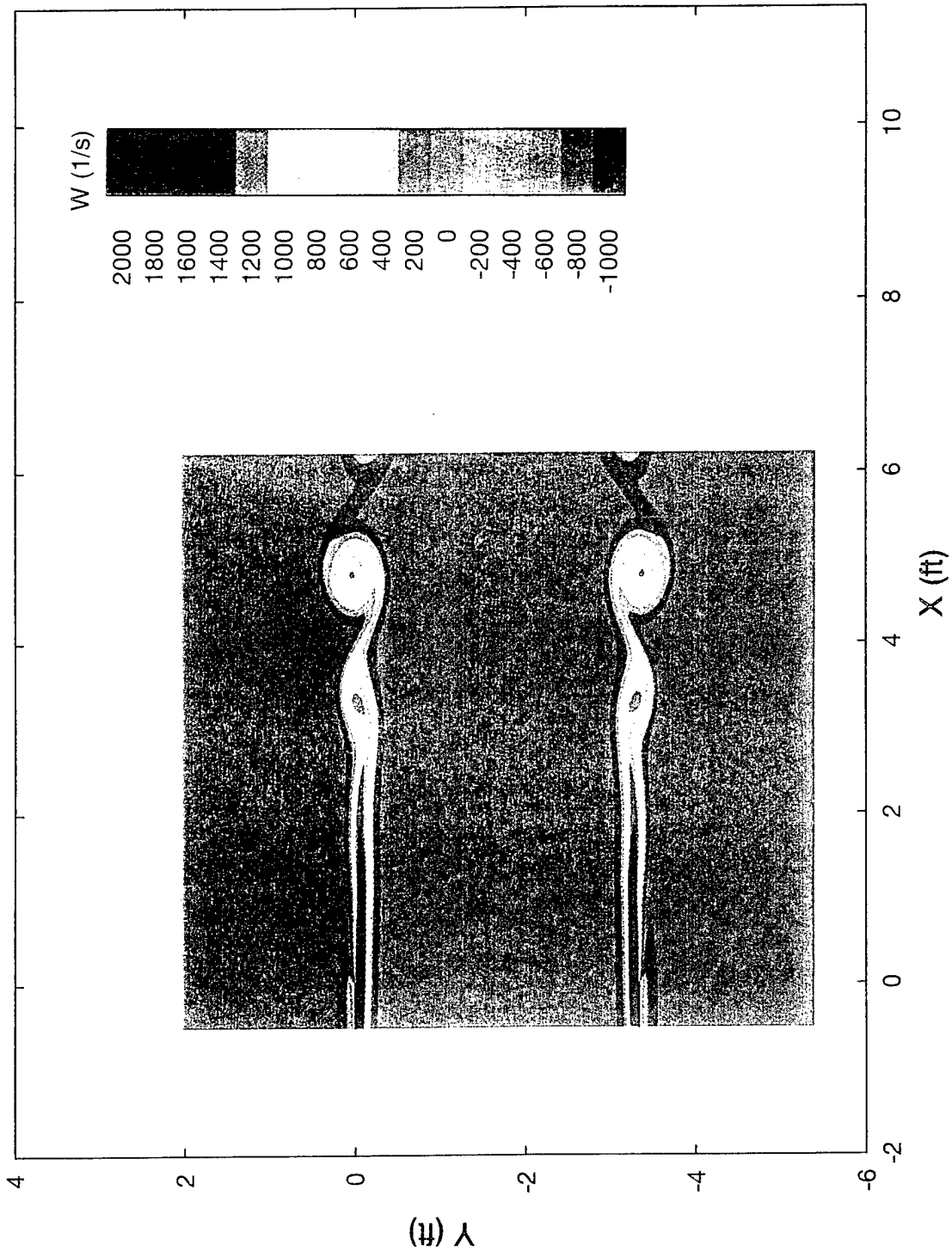

Figure 5.1-12. Vorticity Magnitude for Symmetric Isothermal Case, Minf=0.3, Steady Blowing Amplitude=0.01, Harmonic Forcing Amplitude=0.01.

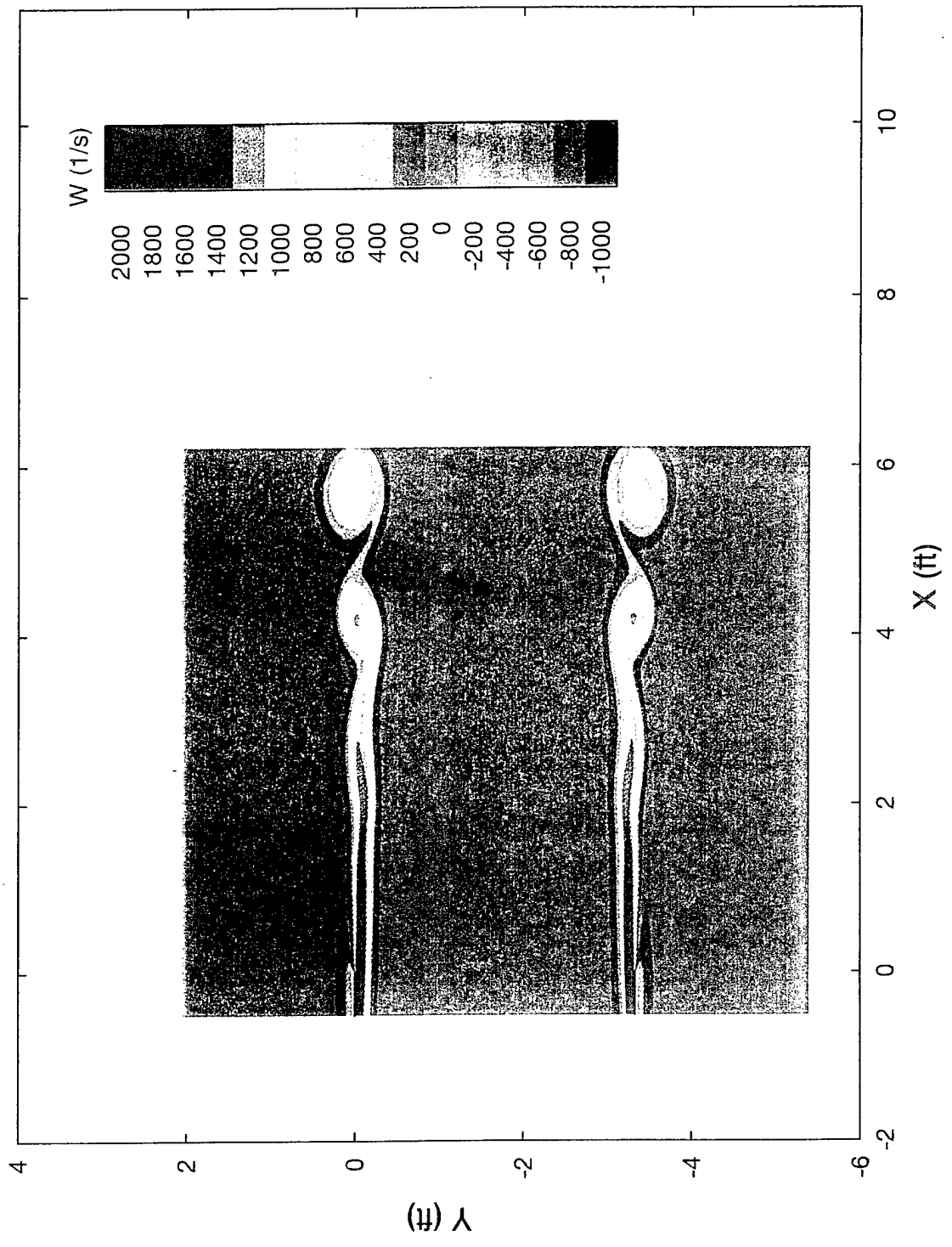

Figure 5.1-13. Vorticity Magnitude for Symmetric Isothermal Case, Minf=0.3, Steady Blowing Amplitude=0.06, Harmonic Forcing Amplitude=0.01.

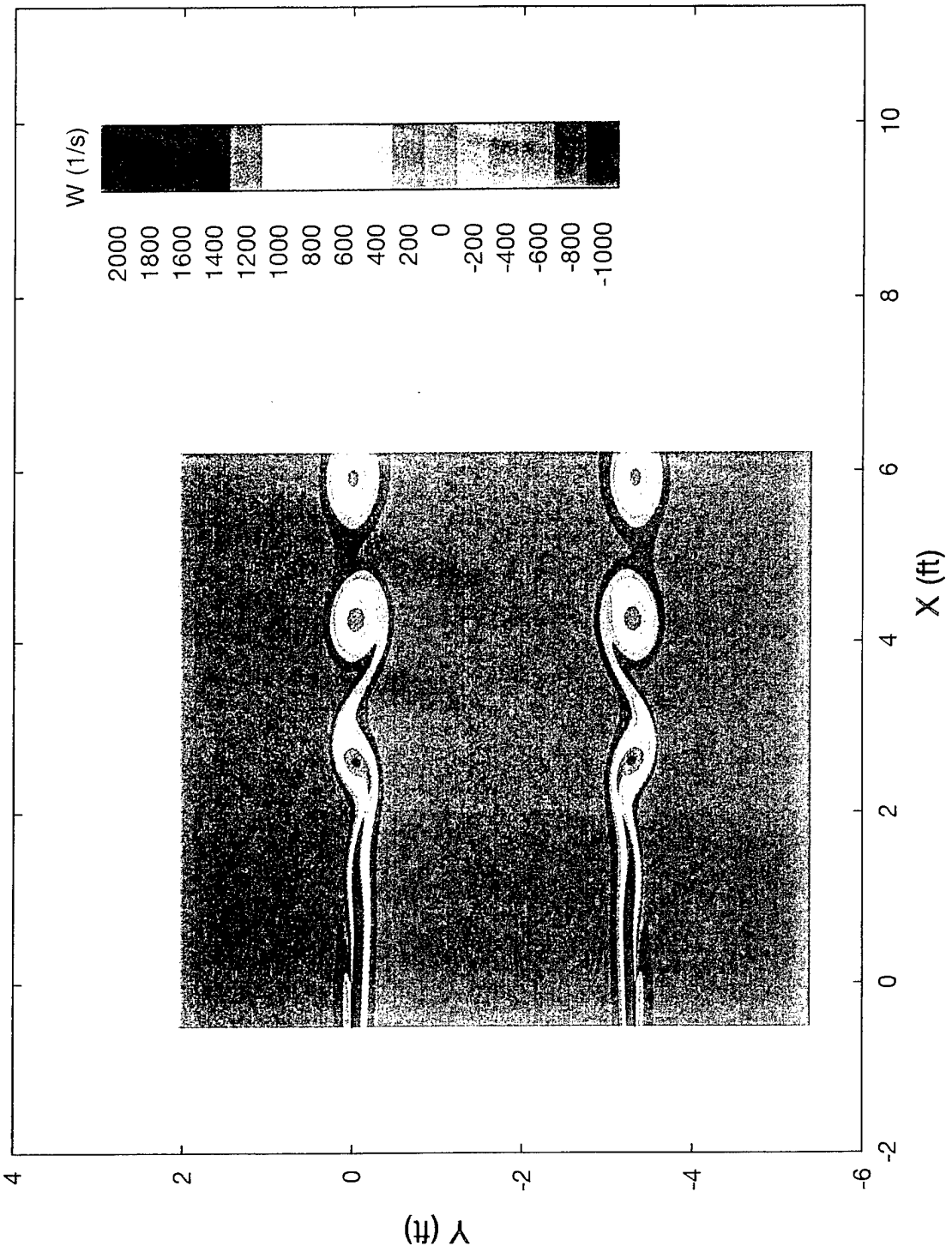

Figure 5.1-14. Vorticity Magnitude for Symmetric Isothermal Case, Minf=0.3, Steady Blowing Amplitude=0.05, Harmonic Forcing Amplitude=0.05.

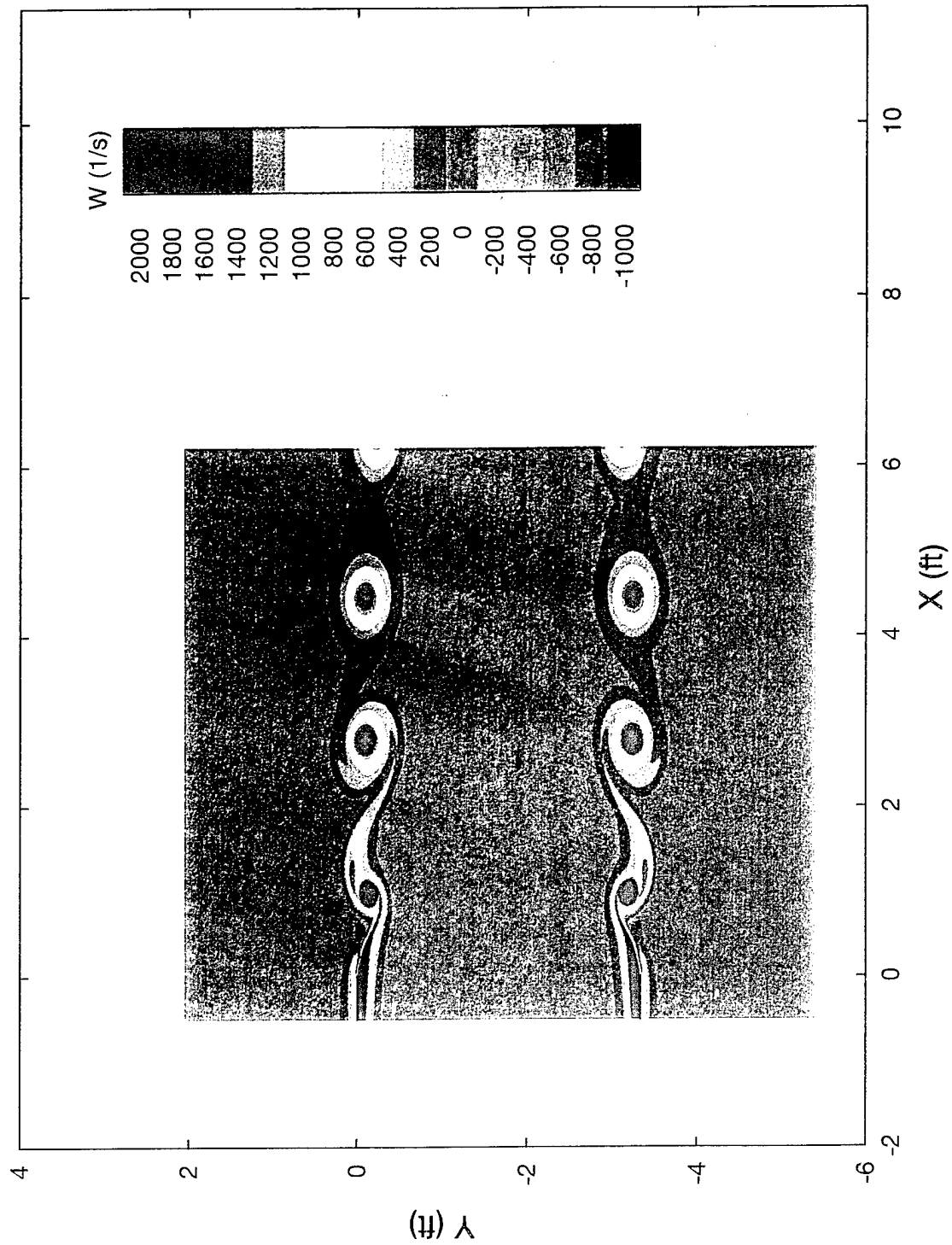

Figure 5.1-15. Vorticity Magnitude for Symmetric Isothermal Case, Minf=0.3, Steady Blowing Amplitude=0.25, Harmonic Forcing Amplitude=0.25.

Figure 5.2-1. Nozzle Lip CFD Grid.

Case	% Change $\delta\omega$ (@4.94")
MP8–BA01–FA01–TI	0.07 *
MP8–BA01–FA01–TH	5.66
MP8–BA06–FA01–TI	0.24
MP8–BA06–FA01–TH	8.80
MP8–BA05–FA05–TI	2.65
MP8–BA25–FA25–TI	0.39
M1P5–BA01–FA01–TI	0.04 *
M1P5–BA06–FA01–TI	0.05 *
M1P5–BA05–FA05–TI	0.001 *
M1P5–BA25–FA25–TI	0.004 *

* Has Reached Stationary State

Table 5.2-1. Relative Stationarity State Condition as Measured by Change in delta-omega.

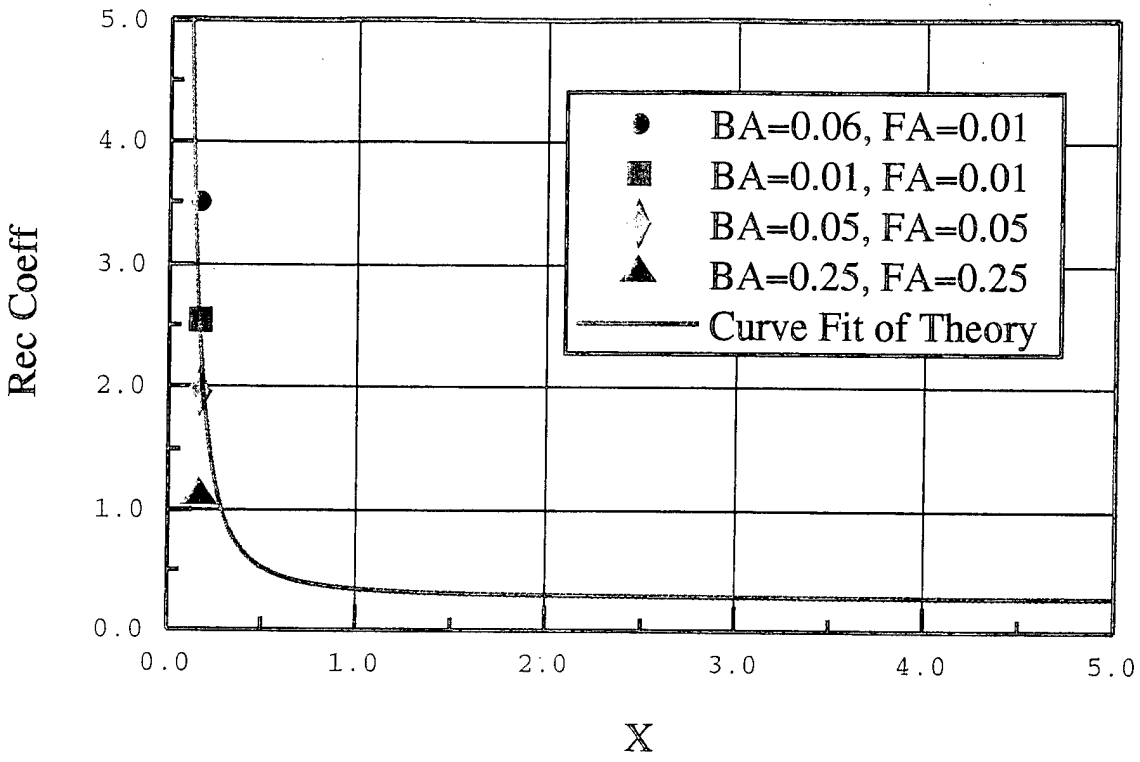

Figure 5.2-2. Comparison of Nonlinear Computation to Linear Theory for Receptivity Coefficient vs Downstream Location (x/wavelength) for Mjet=0.8, Minf=0.15, Isothermal Case.

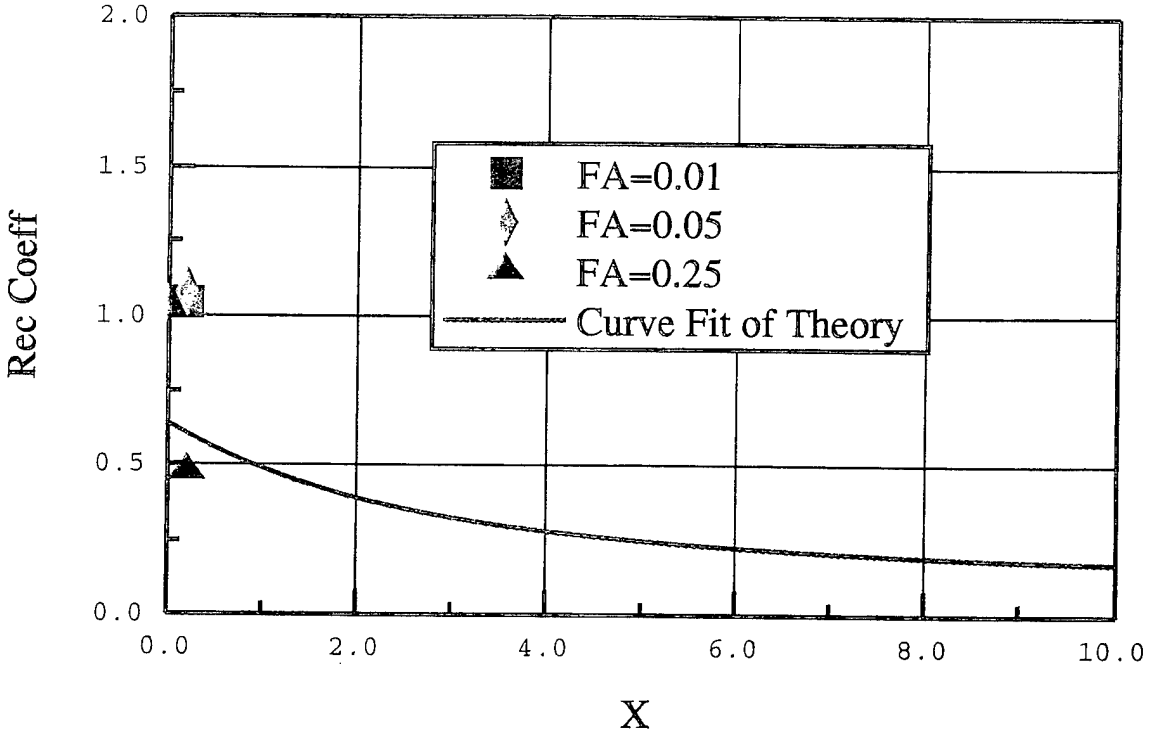

Figure 5.2-3. Comparison of Nonlinear Computation to Linear Theory for Receptivity Coefficient vs Downstream Location (x/wavelength) for Mjet=1.5, Minf=0.15, Isothermal Case.

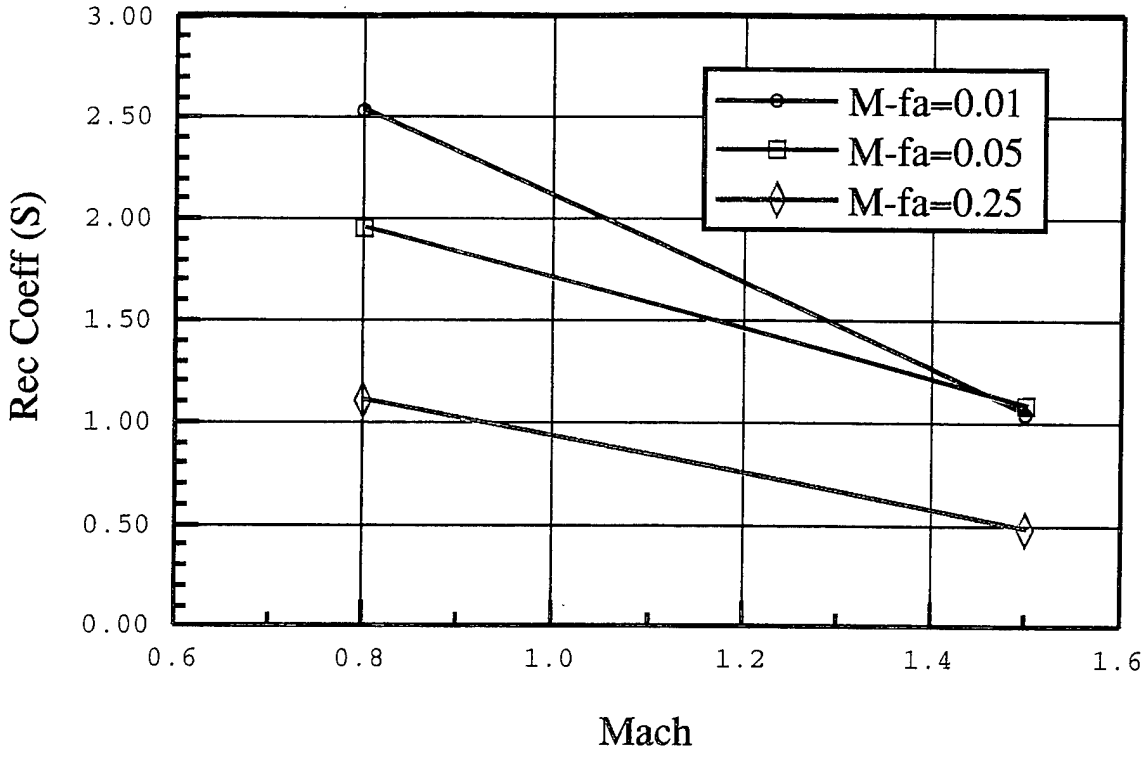

Figure 5.2-4. Receptivity Coefficient vs Jet Mach for Various Harmonic Forcing Amplitudes at Isothermal Conditions.

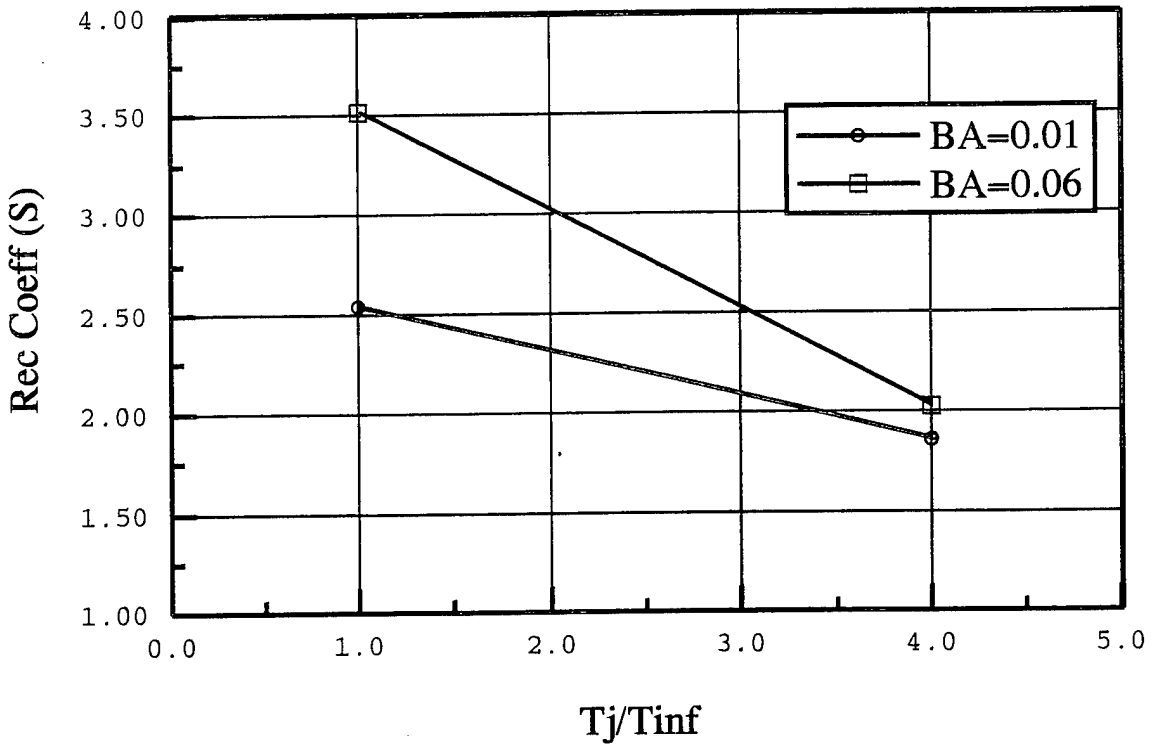

Figure 5.2-5. Receptivity Coefficient vs Jet Temperature Ratio for Various Steady Blowing Amplitudes.

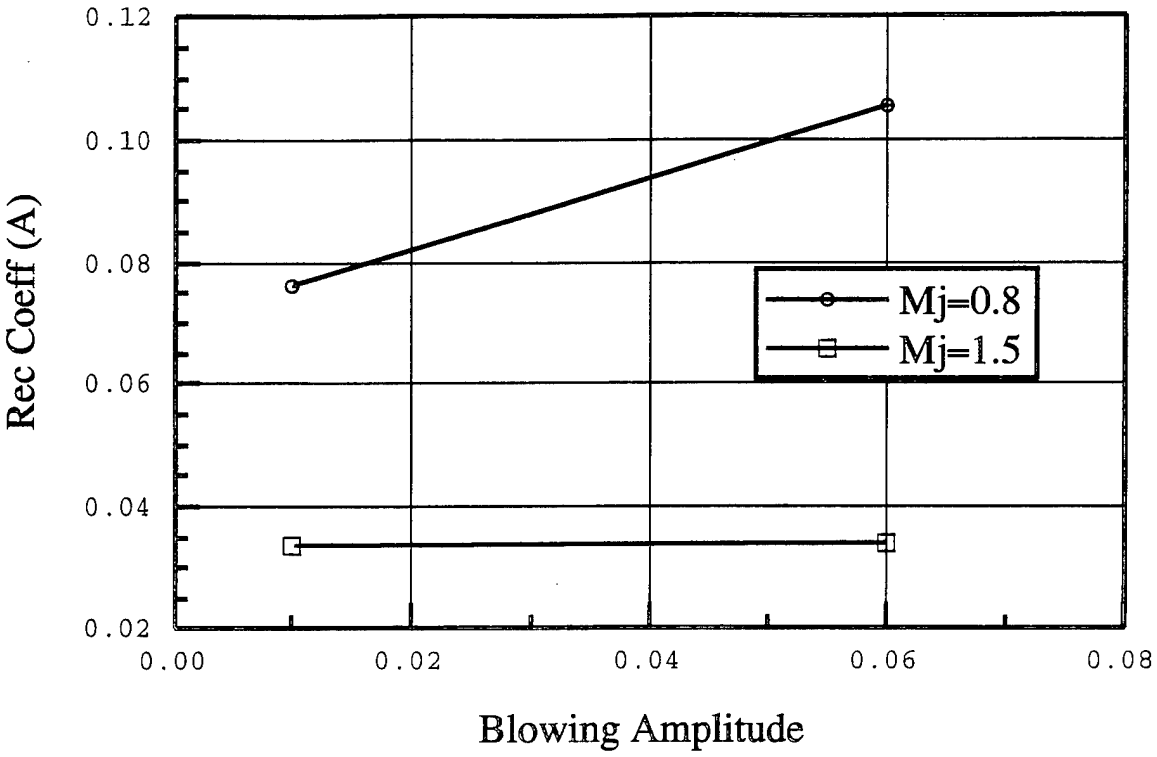

Figure 5.2-6. Receptivity Coefficient vs Steady Blowing Amplitude for Various Jet Mach Numbers.

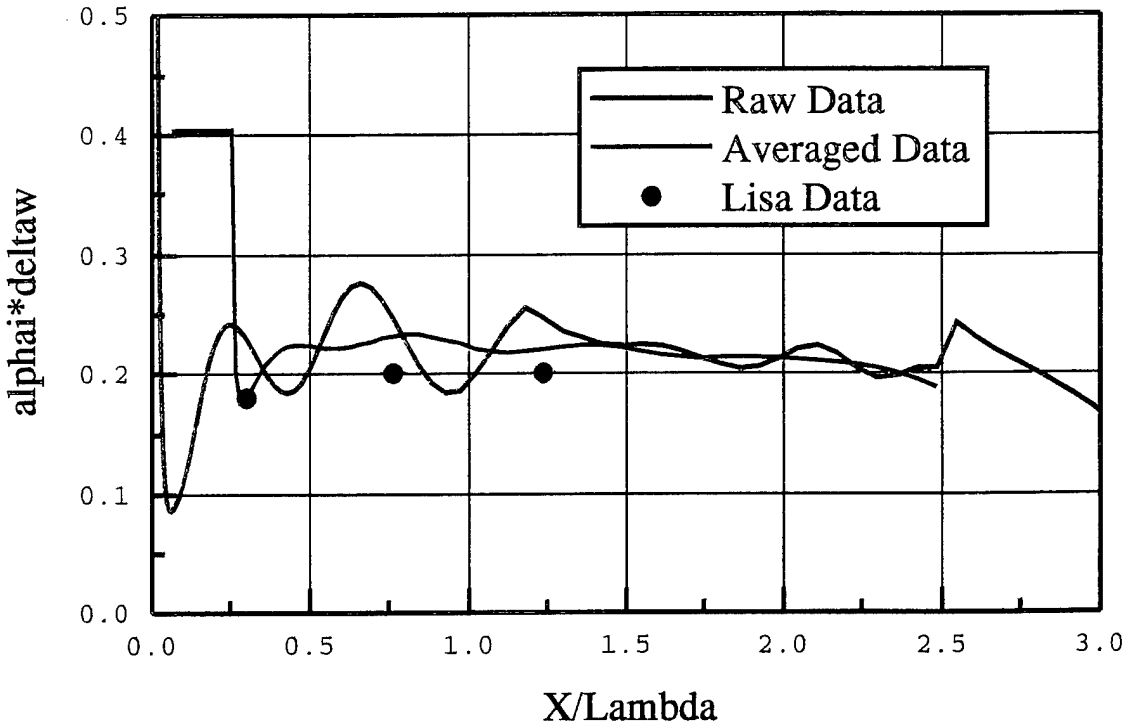

Figure 5.3-1. Comparison of Predicted Growth Rate as Deduced from Nonlinear Computation vs Linear Theory for Mjet=1.5, Steady Blowing Amplitude=0.01, Harmonic Forcing Amplitude=0.01 Isothermal Case.

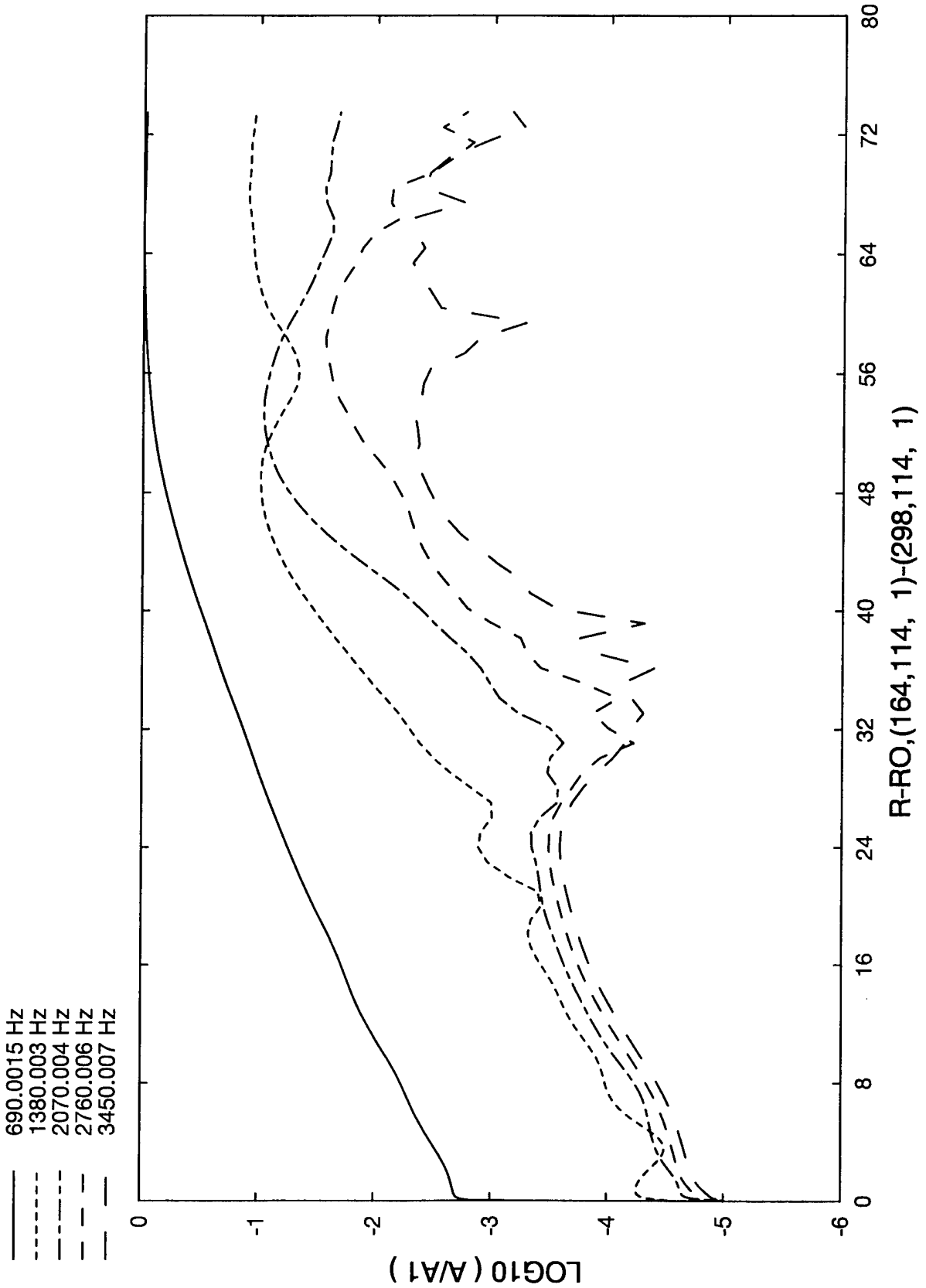

Figure 5.3-2. Fundamental and Higher Harmonic Amplitudes vs Downstream Distance (jet width 40 inches) for Mjet=1.5, Isothermal Case, Steady Blowing Amplitude=0.01, Harmonic Forcing Amplitude=0.01.

6. CONCLUDING REMARKS

In exploring jet receptivity to forcing by periodic injection of mass upstream of the trailing edge, nonlinear computations match linear theory in predicting receptivity coefficients for low forcing levels. Nonlinearity is observed at higher forcing levels, and the receptivity coefficient is found to decrease with increasing forcing amplitude. The onset of nonlinearity is also affected by compressibility considerations as observed in the supersonic flow cases.

Through both experiments and computations, this study characterized the sensitivity of the jet to various forcing and flow parameters and actuator types. Increasing the Mach number from 0.8 to 1.5 reduces the receptivity coefficient by roughly a factor of 2. Increasing the temperature ratio between the jet and the freestream from 1.0 to 4.0 reduces the receptivity coefficient between 25% and 50%. A steady blowing component in addition to harmonic forcing can increase the receptivity coefficient by 40% relative to harmonic forcing alone at a Mach number of 0.8, but the effect was negligible for the supersonic case. Placing the actuator immediately downstream of the nozzle exit increases its effectiveness relative to internal placement. For the external actuator, effectiveness decreases more quickly with increased streamwise distance (normalized by nozzle diameter) than with increased radial distance (normalized actuator slot width) away from the nozzle lip. Additionally, directing the actuator normal to the jet axis produces a greater effect on the shear layer than orienting the actuator at acute or oblique angles. Finally, a consideration of the coupling between a resonant cantilevered actuator and a high speed subsonic jet flow suggests that the acoustic, rather than the fluidic or vortical, component of this excitation source is the dominant factor.

7. REFERENCES

Bechert, D. W. and Stahl, B., 1988, "Excitation of Instability Waves in Free Shear Layers. Part 2. Experiments," *J. Fluid Mech.*, Vol. 186, 63-84.

Goldstein, M.E., 1983, "The Evolution of Tollmien-Schlichting Waves Near a Leading Edge," *J. Fluid Mech.*, Vol. 127.

Kerschen, E. J., 1996, "Receptivity Theory in Compressible Jet Flow Control," AFOSR program final report.

Kerschen, E.J., 1990, "Boundary Layer Receptivity Theory," Applied Mech. Rev., Vol. 43, no. 5, May, 1990.

Morkovin, M.V., 1969, "Critical Evaluation of Transition from Laminar to Turbulent Shear Layers with Emphasis on Hypersonically Traveling Bodies," AFFDL-TR-68-149.

Parekh, D. E., Kibens, V., Glezer, A., Wiltse, J. M., Smith, D. M., 1996a, "Innovative Jet Flow Control: Mixing Enhancement Experiments," AIAA Paper 96-0308.

Parekh, D. E., Bellerose, J., Kibens, V., and Smith, D. M., 1996b, "Enhanced Mixing of Core Exhaust Flow with Active Control," Air Force Research Laboratory final report for Task 8 under Contract F33615-94-C-3000.

Reshotko, E., 1976, "Boundary Layer Stability and Transition," *Annual Rev. of Fluid Mechanics*, Vol. 8.